Determination of extreme sea levels along the Iberian Atlantic coast

André B Fortunato, Kai B Li, Xavier B Bertin, Marta B Rodrigues, Belen Martin Miguez

Determination of extreme sea levels along the Iberian Atlantic coast

André B. Fortunato[1], Kai Li[1], Xavier Bertin[2], Marta Rodrigues[1], BelénMartínMiguez[3]

[1] National Laboratory for Civil Engineering, Estuaries and Coastal Zones Division
Av. do Brasil, 101, 1700-066 Lisbon, Portugal. {afortunato, kaili, mfrodrigues}@lnec.pt

[2]UMR 7266 LIENSs, CNRS - Université de La Rochelle, 2 rue Olympe de Gouges, 17000 La Rochelle Cedex, France. xbertin@univ-lr.fr

[3]Centro Tecnológico del Mar, Vigo, Spain. bmartin@cetmar.org

*Correspondingauthor:*André Fortunato, afortunato@lnec.pt,+351 218443425

LNEC, Avenida do Brasil, 101, 1700-066 Lisbon, Portugal

Abstract

Extreme sea levels along the Atlantic Iberian coast are determined through the development and application of a numerical model for tides and surges, followed by a statistical analysis of the model results.A recent statistical method is assessed using 131 years of data from the Brest tide gauge, and the number of years of data required for an accurate statistical analysis is estimated. The statistical method is extended to consider tide-surge interactions, but they are shown to be small in the study region. The model covers a large portion of the NE Atlantic, with a 250 m resolution in the Portuguese shelf. In the Iberian shelf, RMS errors of tides are of the order of 5 cm, and extreme sea levels are under-estimated by about 10 cm. Differences between sea level statistics obtained from model output and observations are of the order of 5 cm in the study region. Simulation of tides and surges between 1980 and 2010, followed by a statistical analysis of the results, provide the extreme levels along the Iberian Atlantic coast for different return periods. Results reveal the increase of extreme sea levels from south to north and the importance of local effects.

Keywords: Numerical modeling; statistical analysis;tide; storm surge;SELFE

1.Introduction

There is an increasing concern over the flooding of coastal areas. On the one hand, the hazard is increasing due to climate change. Sea level rise directly impacts extreme water levels. In shallow seas, sea level rise can also enhance the tidal amplitude, further affecting extreme water levels (Arns*et al.*, 2015). In some parts of the globe, growing storminess also increases the frequency and severity of extreme events. For instance, Bertin et al. (2013) showed a significant increase of the significant wave height over the whole North Atlantic Ocean during the past century. On the other hand, the vulnerability is also increasing due to the continuous migration of the populations and economic activities to the coast (Nicholls *et al.*, 2007). In Europe, this concern has translated into major legislation (the European directive on the assessment and management of flood risks, 2007/60/EC) and significant research funding in the 7th EU research framework (Quevaullier, 2011) and the new H2020 EU research framework (Perini et al., 2015).

The dominant mechanisms responsible for the flooding vary across the globe. Storm surges dominate in some areas, such as the Gulf of Mexico and the Gulf of Bengal, while tides are also important in many parts of the world (Zhang and Sheng, 2013). Wind waves can also induce a significant setup close to the coast. Bertin*et al*. (2009) estimate this setup at several

tens of cm under energetic waves. Similarly, Bertin*et al.* (2015) estimated the wave setup in harbors sheltered from agitation, in the region of La Rochelle, at 0.10 to 0.20 m for a classical storm with an offshore significant wave height of 7-10 m. Finally, low-frequency, infra-gravity waves can also play a role.As in many other similar studies (e.g., Haigh et al., 2010), the focus here is on the stillwater levels, i.e., the effects of surface waves are ignored.

Determining the hazard from tide gauge data entails major difficulties. Firstly, few tide gauges have time series long enough to provide reliable statistics. For instance, in Portugal, only the Leixões (Araújo*et al.*, 2013), Aveiro (Fortunato *et al.*, 2013), Cascais and Lagos tide gauges have multi-decadal time series. Secondly, some stations are not representative of coastal conditions because they are located inside estuaries. Estuarine water levels differ from sea levels not only due to shallow water processes but also due to the effect of river flow.Thirdly, most annual time series have gaps due to instrument malfunctioning, which severely limit the applicability of statistical methods to determine return periods associated with extreme sea levels. Finally, it is possible that the occurrence of data gaps is not random, but often associated with storms (e.g. Breilh*et al.*, 2014). If this hypothesis was true, as suggested by Figure 1, statistical analyses of extreme sea levels based on tide gauge data would systematically underestimate the true extremes. This problem can be mitigated by combining testimonial with observational data, but this approach can by very time-consuming (Bulteau et al., 2015).

As an alternative to measured sea levels, process-based numerical models avoid the four previous difficulties. Provided adequate computational resources and proper data for their setup, forcing and validation, models can produce long and continuous time series of sea surface height, which can be used to determine the return periods associated with extreme sea levels. This approach has been followed recently by Batstone *et al.* (2013), Zhang and Sheng(2013) andHaigh *et al.* (2014a, b) for the coasts of the UK, western northAmerica and Australia, respectively.

This paper aims at characterizing the extreme sea levels along the Iberian Atlantic coast. Due to the limited number of long tidal records in this area, the extreme levels are determined using 31 years of hindcast simulations of tides and surges. As in the similar studies mentioned above, the focus here is on the still water levels, i.e., the effects of surface waves is ignored. Model results are statistically analyzed to determine sea levels associated with different return periods. To assess the errors introduced by the statistical analysis, the statistical method is first applied and assessed using 131 years of measured water levels from the Brest tide

gauge(France), one of the longest time series in the world (Wöppelmann*et al.*, 2007).Given the difficulty in considering tide-surge interactions in the statistical analyses, the importance of these interactions is briefly assessed.

The paper is organized as follows. Section 2 describes the statistical analysis method, illustrating its application to the Brest data. Section 3 describes the model application and validation and discusses the results.

2. Statistical method: description and assessment

2.1Background

The return periods for extreme sea levels are usually determined using water levels measured at tide gauges. However, measured time series are usually short (typically a few decades) relative to the return periods that need to be determined (typically 10 to 1000 years). This limitation is often aggravated by gaps in the data, associated with instrument malfunctioning. As a result, the tails of the empirical statistical distributions of extreme levels usually have very few data points, thus uncertainties are very high for large return periods. In some cases, the largest storms can appear as outliers in the empirical statistical distributions, casting doubts on their return period (Bardet *et al.*, 2012).

Different methods have been proposed to determine the statistics of extreme sea levels (see Haigh *et al.*, 2010 and Batstone *et al.*, 2013 for recent reviews). Direct methods compute these statistics based on measured extremes. The simpler approach (AMAX) uses only the set of annual maxima, while other approaches (Peak Over Threshold) use several maxima per year (Tawn, 1988; Coles, 2001; Arns*et al.*, 2013). In any case, the number of data points used to construct the statistical distribution remains small, and the uncertainty in the tail of the distribution is large. In an attempt to overcome this shortage,Bernardara*et al.* (2011) and Bardet *et al.* (2012) combined data from several coastal stations in the same region. This approach succeeded in dissipating the doubts about the outliers. However, the dominant physical processes are not necessarily the same at the different stations (e.g., due to different extents of the continental shelf) which casts some doubts on the physical basis of the approach. Furthermore, if the same storm is measured at two nearby stations, the data will not be strictly independent. This limitation was addressed by Weiss et al. (2014).

The Joint Probability Method (JPM, Pugh and Vassie, 1980) constitutes a significant improvement over direct methods by splitting the measured sea level signal into tidal and surge components, and performing independent statistics for each component. The probability

124 distribution of extreme sea levels is then computed through the convolution of the probability
125 distributions of the two components. However, this method has its own shortcomings (Haigh *et*
126 *al.*, 2010):

127 1. It assumes that consecutive hourly measurements of sea levels are independent, which is
128   false as both the tide and the surge signals exhibit strong temporal dependence.

129 2. It assumes that the empirical non-tidal distribution is a sufficiently good estimate of the
130   true distribution. Whilst it is acceptable for most of the range, it is restricted near the
131   extremes, the region of prime interest.

132 3. Confidence intervals cannot be calculated.

133 4. It is more complex than the direct methods because two forms of dependence must be
134   accounted for: seasonality (i.e. larger surges are more prevalent in winter) and tide-surge
135   interaction (i.e. in many regions, non-linear interactions between the tidal and non-tidal
136   components tend to cause surge maxima to occur most frequently at certain phases of the
137   tide).

138 Tawn and Vassie (1989) and Tawn (1992) revised the JPM by fitting an extreme value
139 distribution to the tail of the extremes distribution. Batstone et al. (2013) further improved the
140 JPM by analyzing the skew surge, rather than the instantaneous surge (Skew Surge Joint
141 Probability Method). The skew surge, defined as the difference between the predicted tide and
142 the observations at high tide, is less sensitive to phase lags than the instantaneous surge.
143 However, Batstone *et al.* (2013) found that this approach led to unphysical results in about
144 25% of the stations used in their study. More recently, Mazas et al. (2014) further improved the
145 method. Serafin and Ruggiero (2014) developed a method that splits not only the tidal and
146 surge signal, but also wave runup. While most of the shortcomings of the JPM seem to be
147 overcome, the improved JPM has grown progressively more complicated and difficult to
148 implement.

149 In summary, determining the return periods of extreme sea levels is a difficult task, which
150 entails a significant uncertainty. Significant efforts to address this problem have led to the
151 development and improvement of many methods, with varying degrees of complexity. A
152 consensus on the best method or methods remains to be reached.

153 **2.2 Method description**
154 The method used herein, an extension of the one proposed by Fortunato *et al.* (2013), is akin
155 to the JPM in the sense that the signal is split into various components with a different physical

156　origin. These components are modeled individually, then added together to generate a large

157　set of synthetic yearly time series. An empirical statistical distribution is then determined based

158　on the AMAX method. The large number of synthetic yearly time series (e.g., about 300,000

159　for 20 years of data in Fortunato *et al.*, 2013) mitigates the uncertainty associated with the

160　shortage of data. A very similar approach was proposed by Haigh *et al.* (2014b).

161　The method proceeds as follows. The observed elevation signal, η, is split into several

162　components:

163　　$\eta = \eta(\text{long term}) + \eta(\text{tide}) + \eta(\text{tide/surge}) + \eta(\text{residual})$　　　　　　　　(1)

164　• $\eta(\text{long term})$ is the Mean Sea Level. Here, it is computed as a linear trend in time,

165　　determined by a regression analysis of the annual means of the measured data. Higher

166　　order approximations to the mean sea level dependence on time can easily by adopted.

167　• $\eta(\text{tide})$ is the tidal signal. Tidal constituents are determined through a harmonic analysis of

168　　the long-term time series. The tidal signal can then be reconstructed for any given year by

169　　harmonic synthesis, given the appropriate nodal factors.

170　• $\eta(\text{tide/surge})$ represents the average interaction between tide and surge. This term will be

171　　neglected for the time being, and its evaluation will be discussed in Section 2.5.

172　• $\eta(\text{residual})$ includes all other factors and is thus computed as the difference between the

173　　observed elevation η and the previous terms.

174　The approach proceeds as follows. First, the yearly mean sea level is determined and

175　modeled through a regression function (see Figure 2 for an example for the Brest station). The

176　tidal constituents are determined next by harmonic analysis of the whole series. Finally, hourly

177　residuals are obtained by subtracting the long-term trend and the tidal synthesis from the data.

178　If required, these residuals may be split in distinct components, as will be detailed below. In a

179　second step, yearly time series are synthesized by varying the following factors independently:

180　1) the tide, over a period of 19 arbitrary consecutive years. Using this period allows taking into

181　account the 18.6 years lunar nodal cycle, which has been shown to affect extreme sea levels

182　(e.g., Eliot, 2010). An analysis of the yearly standard deviation of the tidal signal at Brest (not

183　shown) reveals a variability with an amplitude of 10 cm and a period of 19 years.

184　2) the hourly residuals obtained previously, for a user-selected set of years. If these residuals

185　are further split into different components, these are varied independently as well.

186　3) the phase lag between the synthesized tide and the observed residuals. This phase lag,

187   which varies between -15 and +15 days with a time step of 1 hour, allows any observed storm

188   surge to occur at different times in the tidal cycle and in the neap-spring cycle. Hence, extreme

189   sea levels higher than those observed are obtained. While the choice of the phase lag is

190   somewhat arbitrary, a sensitivity analysis showed that using ±30 daysinstead does not affect

191   the results significantly (not shown).

192   The time step mentioned above was set to 1 hour according to the value available in most old

193   tide gauge records. Reducing this time step to a few minutes would probably lead to slightly

194   higher maxima but was not attempted herein.

195   The number of yearly synthetic time series obtained by this procedure is given by the product

196   of the number of consecutive years of tides (19), the number of years of data (up to 131 in the

197   analysis of the Brest data shown below, and 31 for the model results described in the next

198   section) and the number of hours in 30 days (721). The typical number of synthetic time series

199   is thus in the order of 10^5-10^6.

200   The empirical statistical distribution is then obtained by the AMAX method. For consistency,

201   the Mean Sea Level (η(long-term)) is removed from the time series analyzed. To obtain the

202   sea level associated with a given return period for a particular year, the Mean Sea Level for

203   that year (red curve in Figure 2) must be added to the results.

204   This approach overcomes the major problems associated with the JPM listed above. First, the

205   various components are modeled as time series, thus retaining their temporal dependence.

206   This is an advantage over classical convolution methods, which ignore the strong dependence

207   between the water levels at two consecutive times (Haigh *et al.*, 2010). Secondly, the behavior

208   of the extremes is assessed through a convergence analysis, in order to determine how many

209   years of data are required for a converged solution for a particular return period. This analysis

210   allows the estimation of confidence levels. Finally, the seasonality of the tidal and surge

211   signals is taken into account by limiting the phase lag between the two signals to a minimum

212   (15 days). Tide-surge interactions can also be included in the method, as illustrated below.

213   The major limitation of the method is that it cannot assume storm surges higher than the ones

214   present in the input data.

215   **2.3Method assessment**

216   The new method is compared to the AMAX method with a GEV distribution by Fortunato et al.

217   (2013) and to JPM by Lopes and Dias (2015). However, those assessmentsare limited by the

218   short duration of the observational record used (20 years). Herein, one of the world's longest

tidal records is used to provide a more detailed assessment of the new method. The data from the Brest tide gauge are available from the University of Hawaii Sea Level Center (1848-2007) and REFMAR (2008-2011). The data were first screened, and minor problems were corrected. Years with measurement gaps occurring during the maritime winter (October – March) were discarded, as there was the possibility that a significant storm surge went unmeasured. The remaining 131 years were considered in the analysis. For the gaps occurring in the maritime summer, residuals were assumed to be zero since they are unlikely to generate yearly maxima. The harmonic analysis of the observations was performed with the software MAS (Simon, 2007) using about 100 constituents.

A convergence analysis was first performed to determine how the uncertainty of the method varies with the number of years available, and how many years of data are required to obtain reliable values for the return period. As expected, the uncertainty grows with the return periods. Results indicate that with 30-40 years of data, the maximum elevations for return periods of 100 years or less can be determined with an uncertainty of the order of a few centimeters (Figure 3a). However, this result may depend on the particular years used in the analysis. The major recorded storm surge to have hit Brest, in 1987, exceeds all other recorded storms by far (Figure 4). If the year of 1987 is included in the analysis, results change significantly, in particular for the 1000 year return period (dashed lines in Figure 3b). These results indicate that the analysis should preferably be restricted to return periods of 100 years or less. However, because extremes associated with 1000 year return periods are often required for management purposes, they were also included in this study.

The return periods obtained with the new method were compared with the application of the AMAX method to the 131 years of data. A Gumbel distribution was fitted to the empirical cumulative distribution function by a least squares approach, following Haigh et al. (2014b) who found it to provide better results than the GEV distribution. Three alternative approaches were followed to determine the adjustment parameters. The direct fitting of the empirical cumulative density function led to a good agreement of the data for low return periods (up to 10 years) but diverged significantly from the empirical function for larger return periods. In contrast, fitting the empirical return period function led to a good adjustment for return periods above 10 years, but failed for low return periods. The most well-balanced adjustment was obtained by fitting the logarithm of the empirical return period function. Using this adjustment, there is a reasonable agreement between the Gumbel distribution and the empirical functions obtained with the new method (Figure 3a): for return periods between 10 and 1000 years, the

252 discrepancy between the two curves does not exceed 4 cm.The difficulty in finding the best
253 curve-fitting algorithm when adjusting a theoretical distribution to an empirical function
254 constitutes an additional disadvantage of the AMAX method that the method proposed herein
255 avoids.

256 As one of the reviewer pointed out, the statistical method used herein does not address the
257 problem of the small timing errors in observations or tidal predictions. This problem stems from
258 the small phase lags between the tidal predictions and the observations, which can lead to
259 artificially high residuals, hence to an overestimation of the extreme water levels. However,
260 while these phase lags are common in observation records, particularly in old ones, they
261 should not occur in modeled time series. Whatever phase errors may exist in the model time
262 series will be reproduced in the tidal synthesis, thereby avoiding phase differences between
263 the two time series. Hence, this statistical method is particularly suited to time series
264 generated by numerical models.

265 **2.4Time evolution of the sea level extremes**

266 Based on these results, sets of 41 years were analyzed using a running window approach to
267 determine the maximum elevations for different return periods. Results suggest a possible
268 upward trend in the maximum elevation for all return periods, even excluding the effect of the
269 rising mean sea level (Figure 5a). This result would be consistent with the increase in
270 significant wave height found in this region by Bertin*et al*. (2013) for the period 1900-2010.
271 However, for the smaller return periods, this increase is an order of magnitude smaller than
272 the rise in mean sea level (1.27 mm/year at this station, Figure 2): the trends are 0.18 and
273 0.17 mm/year for the 10 and 100 year return periods, respectively. Results also indicate a
274 1.1 mm/year growth trend for the 1000 year return period. However, considering the
275 uncertainty shown above for this return period, this result cannot be considered significant.
276 Close inspection of Figure 5b further shows that this trend is determined to a large extent by
277 the last three data points in the curve, i.e., the ones that are computed using data from 1987.
278 Hence, this analysis does not support the conclusion of a growth of the extreme sea levels at
279 Brest during the last 150 years, apart from the effect of sea level rise which is excluded from
280 this analysis. This result is consistent with a previous study that found that the increase in sea
281 level extremes is mostly a result of sea level rise (Menendez and Woodworth, 2010).

282 **2.5Importance of tide-surge interactions**

283 Tide-surge interactions can represent a significant fraction of the residuals, in particular in
284 shallow areas. For instance,Idier*et al*.(2013) show that these interactions can represent 50%

285   of the maximum surge in the English Channel. Various physical mechanisms have been
286   proposed to explain these interactions. First, tidal propagation can be accelerated
287   (decelerated) by a positive (negative) surge (Horsburgh and Wilson, 2007). This acceleration
288   leads to a phase shift between the measured and predicted tide which translates into positive
289   (negative) residuals during the rising (falling) tide. Secondly, the wind effect (i.e., the wind
290   stress divided by depth in the shallow water equations) is inversely proportional to the water
291   depth. The storm surge will thus tend to be higher at low tide, in particular in shallow areas
292   with a large tidal range (Horsburgh and Wilson, 2007; Antony and Unnikrishnan, 2013). A
293   sensitivity analysis suggests that the first mechanism is small except for very wide and shallow
294   continental shelves, while the latter can lead to tidal modulations of the order of a few tens of
295   centimeters (see Appendix). Other mechanisms have been identified, such as the increase in
296   bottom friction at low tide (Rego and Li, 2010) and advection (Idier *et al.*, 2013). Hence, the
297   relation between the tide and the residual is complex and strongly space-dependent. This
298   relationship is illustrated for Brest in Figure 6, where the number of occurrences of residuals
299   higher than 20, 40, 60 and 80 cm were plotted against the tidal time. The tidal time is defined
300   here as:

301   $\phi = (t-t_1)/(t_2-t_1)$ (2)

302   where t_1 and t_2 are two consecutive times of high water, and *t* is time. The curves on Figure 6
303   were generated using 131 years of data. If the residual was independent of the tidal phase,
304   these curves should be approximately constant. The signals whichappear show that the
305   residuals depend on the tidal phase.The signal is clearest for the lower thresholds, probably
306   due to the higher number of occurrences. Horsburgh and Wilson (2007) present similar signals
307   at other tidal stations. However, these signals vary significantly from station to station,
308   highlighting the complexity of this dependence.

309   As a result of this dependence, the average residual varies along the tidal cycle, and this
310   average increases with the low-frequency surge (Figure 7). The low-frequency surge
311   represents the daily mean sea level, obtained by filtering the observations with a Demerliac
312   filter (Demerliac, 1974). The tide-surge interaction signal also increases with the tidal
313   amplitude, although to a lower extent (not shown). Figure 7 shows that, for a particular
314   location, the knowledge on the phase of the tide provides information on the residual.

315   If the tide-surge interactions are strong, the statistical method described above should take
316   them into account by using the data to model term η(tide/surge) in eq. (1). In the case of Brest,
317   the tide-surge interaction signal is weak even when low-frequency surges are high: about 5 cm

318 for low-frequency surges over 30 cm. Therefore, these interactions should not affect sea level
319 extremes significantly at this site. Mazas*et al.* (2014) also found the impact of considering tide-
320 surge interactions in the evaluation of extreme sea levels at Brest to be negligible. To verify
321 this conclusion, and to illustrate how the method can be adapted to take into account the tide-
322 surge interaction, the term η(tide/surge) is computed as a function of the predicted tidal phase,
323 using a curve similar to the ones in Figure 7 but for all surges. This curveis removed from the
324 values of η(residual) computed previously, then added as a function of η(tide) when
325 reconstructing the synthetic time series.

326 Results show that the maximum elevations for a given return period increase only by a few
327 centimeters at Brest when the tide-surge interaction is considered(Figure 5b). This increase is
328 associated with the average residual at high tide, which is positive (Figure 7). However, this
329 average residual can be negative at other places (Horsburgh and Wilson, 2007), so it cannot
330 be assumed that considering this effect will always increase the maximum elevations.

331 Statistical methods to analyze extreme sea levels have typically dealt with the tide-surge
332 interactions by analyzing the so-called skew surge (e.g., Bardet *et al.*, 2011). The skew surge
333 is the difference between the maximum observed sea level during a tidal cycle and the
334 corresponding predicted high tide. The underlying hypothesis is that the skew surge is not
335 affected by phase lags in the observed tides. Hence, the skew surges would be independent
336 of time of arrival of the storm surge relative to the tide. However, Idier*et al.* (2012) showed that
337 the skew surges can also depend on the tidal amplitude, hence do not eliminate the tide-surge
338 interaction effects. The approach introduced herein appears therefore as an alternative to take
339 the tide-surge interactions into consideration.

340 Even though this approach provides a possible way to take tide-surge interaction into account
341 in the determination of extreme sea levels, it must be recognized that it is cumbersome, as the
342 effects of tide-surge interactions on the sea levels vary strongly with the location. Also, the
343 tide-surge interaction could be easily modeled in Brest because the signal is very clear.
344 However, most stations and hindcast databases have much shorter records, which may result
345 in more noisy signals, more difficult to model.

346 For the particular case of Brest, in spite of the wide continental shelf, a macro-tidal range and
347 strong surrounding tidal currents, the effect of tide-surge interactions on extreme sea levels is
348 small. In the Iberian Atlantic coast, these effects have been shown to be very small due to the
349 narrow continental shelf (Fanjul et al., 1998) and will be neglected henceforth.

3. Extreme sea levels along the Iberian Atlantic coast

3.1 Study site

The Iberian Atlantic coast extends from the Strait of Gibraltar, in the south, to the Spanish-French border in the north (Figure 8). The continental shelf is about 20-70 km wide. Tides are semi-diurnal. The amplitude of M2 is about 1.0 m in most of the south and western coast, and increases to 1.4 m along the north coast (Fortunato et al., 2002). Storm surges increase from south to north. For a 100 year return period, the storm surges at four coastal stations along the Portuguese coastwere estimated to be between 70 and 90 cm (Andrade, 2006). These values could be slightly underestimated, as an observed value above 1 m was reported in Aveiro (Fortunato et al., 2013). The western and northern coasts have very energetic wave regimes, as they are directly exposed to the waves coming from the Atlantic Ocean. For instance, the 90th percentile of the offshore Hs varies in the range 4-6 m (Dodet et al., 2010).Significant wave heights (Hs) grow from south to north.

The coast has many low-lying areas, including sand spits and barrier islands that are occasionally overtopped and breached. Many areas surrounding major estuaries and lagoons are also close to mean sea level. For instance, the zone surrounding the Ria de Aveiro between 0 and 4 m above mean sea level has an area of about 160 km^2 (Fortunato et al., 2013). There are historical records of severe damages and casualties associated with storm surges in the Portuguese coast. Pereira and Coelho (2013) report 86 episodes of overtopping and 21 episodes of dune destruction by the sea since 1850 in the Aveiro region alone. Several episodes of inundation in the Ria Formosa and in the Tagus estuary are illustrated in Carrasco et al. (2012) and in Tavares et al. (2015), respectively.In February 15, 1945, a major storm hit the Iberian coast at high tide and caused extensive damage (Muir-Wood, 2011; Freitas and Dias, 2013): downtown Lisbon and Sesimbrawere flooded, several ships sank, railways and houses were destroyed, and a new inlet, 1000 m wide, was breached in the Ria Formosa. At least 130 casualties were reported in Portugal and Spain, although not all can be attributed to flooding.If this storm occurred today, the estimated damage in the Iberian Peninsula would exceed 6 billion euros (Muir-Wood, 2011). More recently, the damages caused by the 2014 Hercules storm caused tens of millions euros worth of damage along the Portuguese coast.

3.2Model description and application

The hydrodynamics were simulated with the community model SELFE (Zhang and Baptista, 2008), a semi-implicit finite element shallow water model, which targets cross-scale applications. The implicit nature of the model and the use of an Eulerian-Lagrangean method for advection avoid Courant number restrictions, allowing the use of large time steps. SELFE

384   is the core of a suite of community models, which include modules for ecosystem dynamics

385   (Rodrigues *et al.*, 2009, 2012), fecal contamination dispersion (Rodrigues *et al.*, 2011), oil spill

386   dynamics (Azevedo*et al.*, 2014), sediment transport and morphodynamics (Pinto *et al.*, 2012,

387   Dodet, 2013) and wave-current interaction (Bruneau*et al.*, 2011, Roland *et al.*, 2012). The

388   simulations were performed with the two-dimensional version of Zhang *et al.* (2011), providing

389   the free-surface elevations and depth-averaged velocities.

390   The model covers the domain between latitudes 26º and 70º N, and from longitude 19.5ºW to

391   the European coastline (Figure 8). The grid has about 150,000 nodes and its resolution is

392   highest along the Portuguese coast, where it reaches 250 m, and in the western coast of

393   France. The bathymetry is mostly taken from EMODnet (www.emodnet-bathymetry.eu), with

394   small corrections and add-ons. The model is forced by tides, wind and atmospheric pressure.

395   Tidal boundary conditions (18 constituents: Z0, O1, K1, P1, Q1, M2, S2, N2, K2, 2N2, MU2,

396   NU2, L2, M3, M4, MS4, MN4, M6) are taken from the regional tidal model of Pairaud*et al.*

397   (2008) and tidal potential is included inside the domain (11 constituents: SSA, MM, MF, O1,

398   K1, P1, Q1, M2, S2, N2, K2). Winds and atmospheric pressure from CFSR reanalysis (Saha*et*

399   *al.*, 2010), with a 1 hour resolution, are used to force the model inside the domain, and the

400   inverse barometer effect is added at the open boundaries.The wind stress is computed with a

401   wind-dependent drag coefficient following Pond and Pickard (1998). The time step is set to

402   300 s.

403   The model was not calibrated. A preliminary sensitivity analysis showed that the errors tended

404   to decrease slightly in the northern European stations for larger values of the Manning

405   coefficient, but were insensitive to this parameter to the south of France. Hence, a constant

406   Manning coefficient of 0.03 m$^{1/3}$/s was used. The diffusion coefficient was set to zero.

3.3 Model assessment

408   Several error measures were used to assess the model performance. Root mean square

409   (RMS) errors were used to analyze the performance of the tidal model alone. RMS errors were

410   computed from observed and modeled time series synthetized with the major semi-diurnal

411   (M2, S2, N2) and diurnal(O1 and K1)constituents.The normalized variance of the difference

412   between model and observations provides an integral measure of model performance (Zhang

413   and Sheng, 2013). This error norm is defined as:

414    $\gamma^2 = \text{Var}(O-M)/\text{Var}(O)$ (5)

415   whereVar represents the variance, and O and M stand for the observations and predictions,

416   respectively. The peak error range was used to quantify the ability of the model to capture the

417   peak elevations. The peak error range is defined as the maximum positive and negative

418   differences between the observed and the modeled high tides. Note that the observed and

419   modeled high tides may not occur exactly at the same instant, so phase errors do not affect

420   the peak range. Finally, statistics of extreme sea levels were also compared to those derived

421   from observations or other models, where available.

422   The model was first validated for tides. Root mean square errors for the 5 representative

423   constituents at stations in the southern part of the domain are typically smaller than 5 cm

424   (Figure 9a). These errors are smaller than or equivalent to those presented in previous similar

425   applications (Fortunato *et al.*, 2002, 2011).These absolute errors are higher inthe French

426   coast, possibly due to the higher tidal ranges.

427   The full tide and surge model was validated next for the 2009-2010 winter. This period was

428   selected because it was a particularly violent winter. In February, the Xynthia storm generated

429   surges over 1.5 m in the south-western French coast, killing 47 people and causing an

430   estimated 1.5 billion euros of damage (Bertin*et al.*, 2012). The same storm had significant

431   impacts in the Portuguese coast as well (Guerreiro*et al.*, 2015).

432   Normalized errors (Figure 9b) and peak errors (Figure 9c) show that the model captures the

433   variance and the peaks of the measured signal in most of the domain (i.e., in the Iberian

434   Peninsula and further south): the normalized variance γ^2 is smaller than 3% and the peak

435   errors are typically below 20 cm.However, themodel accuracy degrades progressively along

436   the French western coast.

437   This varying spatialaccuracy of the model can be partly attributed to the coarser grid resolution

438   in the northern part of the domain, which was included to simplify the definition of the boundary

439   conditions. However, the grid is also coarse in the Macaronesia region, where errors are very

440   small. Hence, the variability of the model errors should be mostly attributed to the different

441   physical processes that dominate the generation of extreme sea levels.

442   Storm surges are generated by both strong wind and low atmospheric pressure. The wind

443   effect is amplified by extensive shallow areas because the wind stress is divided by depth in

444   the shallow water equations. In contrast, the atmospheric pressure term in the governing

445   equations does not depend on depth. As a result, the relative importance of the two forcing

446   agents on the storm surge can differ significantly depending on the extent of the continental

447   shelf. In the present model application, the continental shelf is much wider in the northern part

14

448 of the domain than in the southern part (Figure 8). Hence, the wind stress should play a more

449 important role in the generation of storm surges in the northern part of the domain than in the

450 south.In the Iberian Atlantic shelf, the wind contribution to the storm surges was estimated at

451 about 30% (Fanjul*et al.*, 1998). Since atmospheric models reproduce air pressure better than

452 wind velocity, the difference in the dominant forcing term should also help explaining the

453 variability of the model accuracy.In particular, the resolution of the wind fields used herein is

454 relatively coarse, which tends to smooth the extreme events. For instance, Stopa and Cheung

455 (2014) show that CFSR underestimates the higher wind speeds. This limitation of wind models

456 can be overcome using parametric winds (e.g., Zhangand Sheng, 2013), but this approach

457 was mostly applied to tropical cyclones and was not followed herein. Also, the evaluation of

458 wind stress depends on an empirical drag coefficient, which can introduce additional errors for

459 specific storms. The errors for the Xynthia storm in La Rochelle illustrate these errors. The

460 model underestimates the peak sea level duringXynthia by about 70 cm (Figure 9c), of which

461 about 0.5-0.6 m can be attributed to the representation of the surge. The inability of the model

462 to reproduce the Xynthia storm in the French coast in general, and at La Rochelle in particular,

463 is due to the very specific track of that storm (Bertin*et al.*, 2012). Contrary to most storms in

464 this region, the Xynthiatrack was SW-NE. Xynthia hit Europe first in the north of Spain, then

465 continued over the Bay of Biscay, where it generated the waves that hit the French coast. The

466 very high steepness of these young waves increased the transfer of momentum from the

467 atmosphere to the ocean, exacerbating the wind setup. The adequate representation of the

468 Xynthia storm surge in the French coast thus requires the coupling between a wave and a

469 circulation model, to include the effects of waves on the surface stress (Bertin*et al.*, 2012).

470 Hence, the present implementation of the model significantly underestimates the Xynthia

471 storm surge in the French coast. Since storms following this particular track generate some of

472 the highest surges along this coast (Breilh*et al.*, 2014), the model will underestimatesome

473 major extreme sea levels in the French coast.

474 Finally, the return periods associated with extreme levels at four stations were computed with

475 the model results and compared to a similar evaluation using data fromCascais, Aveiro and

476 Brest (Figure 9d). Results indicate uncertainties in the extreme sea levels of the order of 5 cm

477 at the Iberian stations: up to 8 and 15 in Cascais and Aveiro, respectively. Considering the

478 analysis of the Brest data, this error is of the same magnitude as the uncertainty associated

479 with the use of only 31 years of data. Again, and as for the peak errors, the discrepancy

480 between the model and data statistics is higher at the Brest station (10-20 cm). Results at

481 Bilbao were also compared with those performed by Marcos et al. (2012) with a different

482 model and a different statistical approach. The small discrepancies between the two, up to

483 8 cm, provide further confidence in the present approach.

484 The comparison between the statistics based on the model and the observations suggests that

485 the model tends to underestimate the extreme sea levels. This underestimation occurs in

486 Cascais, Brest and in Aveiro for the higher return periods. This behaviour is probably due to

487 the lack of wave setup in the model.

488 As a final assessment of the model, Figure 10 compares hourly residuals computed from

489 model results observations. The event corresponds to a storm that hit the Portuguese coast on

490 November 7 1982, when offshore significant wave heights reached 8 m and the storm surge

491 exceeded 50 cm.

492 The model correctly reproduces both the amplitude and phase of the surge in Cascais, with a

493 RMS error of 7 cm between days 306 and 314 (Figure 10). At Aveiro, the model is less

494 accurate, with a RMS error of 15 cm. The model underestimates the surge at Aveiro, which is

495 consistent with the absence of wave setup in the model. Also,the larger errors at Aveiropartly

496 arise from the semi-diurnal signal in the residuals computed from observations,which is absent

497 in the residuals determined with the model. This semi-diurnal signal can have two possible

498 sources. The signal could be due to tide-surge interactions associated with the strong tidal

499 currents in the Aveiro tidal inlet, which are not represented by the model. Further work is

500 required to investigate the possibility of tide-surge interactions at these small scales.Also, the

501 semi-diurnal signal could be due to the small phase lags between the observations and the

502 tidal predictions. If this hypothesis is correct, then the discrepancies between the residuals

503 obtained from the model and from the observations do not correspond to model errors.

504 In summary, the model proved to be highly reliable to analyze extreme sea levels in the

505 southern part of the domain, even though its accuracy degrades further north. Hence, the

506 analysis of model results concentrates on the Iberian Atlantic shelf.

507 **3.4Results and discussion**

508 Hourly model results for the period 1980-2010 along the Iberian coast were used to determine

509 extreme sea levels relative to local mean sea level for different return periods.Figure 11

510 illustrates these results for a return period of 100 years. The harmonic analysis is performed

511 on the fly by the model itself in a one-year simulation forced by tides alone. Only the 21 forcing

512 constituents and two major additional compound tides (MSf and 2MS6) are considered.

513 Otherwise, the statistical analysis proceeds as described in Section 2.

514 Results show that extreme sea levels increase significantly from south to north in this

region:the difference between the extreme sea levelsin the south of Spain (Gibraltar) and the south of France (St. Jean de Luz) is of the order of 2 m. This growth is mostly due to the northward increase of tidal ranges in this area:model results show an increase in maximum tidal elevations between the south and the north of Spain exceeding 1 m (Figure 12).

At smaller spatial scales, results reveal strong increases of extreme sea levels in some sheltered areas. For instance, the 100-year extreme sea level can increase by 0.2-0.3 m from the mouth to the head in several funnel-shaped rias in the north of Spain (Figure 13). This behaviour confirms the importance of basing extreme sea level analyses on model results rather than coastal stations, which may not be representative of regional levels.

The differences between extreme sea levels for return periods of 20 and 1000 years appear modest, increasing from about 0.1 m in the south of the Spain to 0.35 m in the south of France (Figure 14). In the Portuguese coast alone, the extreme sea level for a 1000 return period is only 18 to 25 cm higher than for a 20 year return period. By using the 100 year return period for all planning purposes, the uncertainty associated with the choice of the return period is of the order of 10 cm at most. This uncertainty is small in absolute terms, and is of the same order of the model errors, and of those associated with the choice of the statistical method. Hence, even though the European directive on the assessment and management of flood risks (2007/60/EC) recommends that inundation maps are constructed for three different return periods (to be specified by each member state), these differences suggest that, for many engineering purposes, a single return period can be adopted in the Portuguese coast.Similarly, a single return period could be used in southern Atlantic coast of Spain.

In spite of the good accuracy of the model indicated by the model-data comparisons presented above, some processes which are not included in the model may introduce relevant errors in some areas. First, the model used herein does not include waves and their effects on the mean flow. Hence, both wave setup and infra-gravity waves are implicitly neglected. These effects can increase extreme sea levels significantly in some areas. Also, coastal inundation is prevented in this application, as the grid does not extend into land. Bertin*et al.* (2014) showed that this approach can artificially increase the sea level at the coast, as the water that would otherwise flood the land accumulates at the boundary. Hence, results may both over- and under-estimate extreme sea levels at different locations.

4. Summary and conclusions

The extreme sea levels along the Iberian Atlantic coast were determined for different return periods using a combination of multi-decadal hindcast simulations of tides and surges with a

548 statistical analysis.

549 The statistical method was validated using 131 years of data from the Brest tide station. The

550 method was extended to take into account tide-surge interactions, and it was shown that the

551 effect of these interactions on extreme sea levels is negligible in the particular area analyzed.

552 Results suggest that with 30-40 years of data, the maximum elevations for return periods

553 below 100 years can be determined with an uncertainty of the order of a few centimeters.

554 The model covers a large portion of the NE Atlantic, and has a resolution of 250 m in the

555 Portuguese shelf. The model was extensively validated for tides, surges and extreme sea

556 levels. In the Iberian Atlantic shelf, RMS errors of tides are of the order of 5 cm, and the model

557 under-estimates extreme sea levels by about 10 cm. More importantly, sea level statistics

558 computed with the model results agree with those computed with tide gauge data.

559 Results provide a detailed picture of the extreme sea levels along the Iberian Atlantic coast.

560 Extreme sea levels grow significantly from south to north, due to the increase in both tidal

561 range and storm surges. Extreme levels can also increase locally by tens of centimetres in

562 funnel-shaped rias. The differences between extreme sea levels for 20 and 1000 year return

563 periods are modest, in particular in the Portuguese coast and in the southern Atlantic coast of

564 Spain. These small differences suggest that for many engineering purposes it is sufficient to

565 analyse a single representative return period in these regions.

566 The main limitation of the model is that waves are not modelled, thus wave setup and infra-

567 gravity waves are neglected. Hence, future efforts should be directed towards reducing this

568 source of errors. As a first approximation, combining regional wave hindcasts (e.g., Dodet*et*

569 *al.*, 2010) with empirical relations between wave characteristics and wave-induced setup (e.g.,

570 Holman, 1986; Stockdon*et al.*, 2006) can improve the model results at acceptable

571 computational costs.

572

Acknowledgments

586

Appendix: assessment of two tide-surge interaction mechanisms

Two possible mechanisms for tide-surge interaction are briefly assessed. For simplicity, we consider a tide and a surge propagating along a continental shelf with a constant depth H.

The first mechanism notes that the celerity of the tide can be enhanced or reduced by a positive or negative surge, respectively (Horsburgh and Wilson, 2007). The resulting phase shift between the measured and predicted tide translates into residuals. This phase shift can be estimated as:

$$\Delta\phi = \frac{L}{T}\left(\frac{1}{c} - \frac{1}{c'}\right) \tag{A.1}$$

Where L is the extent of the continental shelf, T is the tidal period, and $c=(gH)^{0.5}$ and $c'=(g(H+s))^{0.5}$ are the celerity of the tide in the absence or in the presence of a surge s, respectively. The difference between the predicted tide (without phase shift) and the observed tide (with a phase shift $\Delta\phi$) constitutes the tide-surge interaction effect. However, an analysis of these effects shows that they are negligible except for very wide and shallow shelves (Figure A. 1).

Another mechanism of tide-surge interaction is the effect of total water depth on the depth-averaged wind stress. The wind forcing (i.e., the wind stress divided by depth in the shallow water equations) is inversely proportional to the water depth. The storm surge will thus tend to be higher at low tide, in particular in shallow areas with a large tidal range. The difference between wind setup at low and high tide ($\Delta\eta$) can be estimated as:

$$\Delta\eta = \frac{LC\rho_a W^2}{\rho g}\left(\frac{1}{H-A} - \frac{1}{H+A}\right) \tag{A.2}$$

where C is the empirical drag coefficient, W is the wind speed, A is the tidal amplitude, ρ_a and ρ are the air and water densities, respectively, and g is gravity. Figure A. 2 shows that, for long and shallow continental shelves, this effect can reach 0.5 m.

References

Andrade, C.,Pires,H.O.,Silva,P.,Taborda,R.,Freitas,M.C.,2006. Zonas Costeiras, in: Santos, F.D. andMiranda,P.(Eds.),*Alterações climáticas em Portugal. Cenários, impactes e medidas de adaptação — Projecto SIAMII*.Gradiva,Lisboa, in Portuguese.

Antony, C.,Unnikrishnan, A.S.,2013. Observed characteristics of tide-surge interaction along the East coast of India and the bay of Bengal, *Estuarine, coastal and Shelf Science*, 131: 6-11.

Araújo, I.B., Bos, M.S.,Bastos, L.C.,Cardoso, M.M.,2013. Analysing the 100 year sea level record of Leixões, Portugal, *Journal of Hydrology*,481: 76-84.

Arns, A., Wahl, T., Haigh, I.D, Pattiaratchi, C., Jensen, J., 2013.Estimating extreme water level probabilities: a comparison of the direct methods and recommendations for best practice, *Coastal Engineering*, 81: 51-66.

Arns, A., Wahl, T., Jensen, J., 2015.The impact of sea level rise on extreme water levels in the northern part of the German Bight, *Coastal Engineering*, 96: 118-131.

Azevedo, A., Oliveira, A.,Fortunato, A.B.,Zhang, J.,Baptista,A.M., 2014. A cross-scale numerical modeling system for management support of oil spill accidents, *Marine Pollution Bulletin* 80, 1-2: 132 - 147.

Bardet, L., Duluc, C.-M., Rebour, V. and L'Her, J., 2011. Regional frequency analysis of extreme storm surges along the French coast, *Nat. Hazards Earth Syst. Sci.*, 11, 1627-1639.

Batstone, C., Lawless, M., Tawn, J., Horsburgh, K., Blackman, D., McMillan, A., Worth, D., Laeger, S., Hunt, T., 2013. A UK best-practice approach for extreme sea-level analysis along complex topographic coastlines, *Ocean Engineering*, 71: 28-39.

Bernardara, P., Andreewsky, M.,Benoit,M., 2011.Application of regional frequency analysis to the estimation of extreme storm surges, *J. Geophys. Res.*, 116, C02008, doi:10.1029/2010JC006229.

Bertin, X., Fortunato, A.B, Oliveira, A., 2009. A modeling-based analysis of processes driving wave-dominated inlets.*Continental Shelf Research*, 29/5-6: 819 - 834.

Bertin, X., Bruneau, N.,Breilh, J.F.,Fortunato, A.B.,Karpytchev,M.,2012.Importance of wave age and resonance in storm surges: the case Xynthia, Bay of Biscay. *Ocean Modelling*, 42, 16-30.

Bertin, X., Prouteau, E., Letetrel, C., 2013. A significant increase in wave height in the North Atlantic Ocean over the 20th century, *Global and Planetary Change*, 106: 77-83

Bertin, X., Li, K., Roland, A., Zhang, Y.J., Breilh, J.F., Chaumillon, E. 2014. A modeling-based analysis of the flooding associated with Xynthia, central Bay of Biscay, *Coastal Engineering*, 94: 80-89.

Bertin, X., Li, K., Roland, A., Bidlot, J.R., 2015. The contribution of short-waves in storm surges: two case studies in the Bay of Biscay, *Continental Shelf Research*, 96: 1–15.

Breilh, J.F., Bertin, X., Chaumillon, E., Giloy, N., SauzeauT., 2014. How frequent is storm-induced flooding in the central part of the Bay of Biscay?,*Global and Planetary Change*, 122: 161-175.

Bruneau, N., Dodet, G., Bertin, X., Fortunato, A.B.,2011. Development of a three-dimensional coupled wave-current model for coastal environments, *Journal of Coastal Research*, Special Issue 64, 986 - 990.

Bulteau, T., Idier, D., Lambert, J., Garcin, M., 2015. How historical information can improve estimation and prediction of extreme coastal water levels: application to the Xynthia event at La Rochelle (France), *Natural Hazards and Earth System Science*, 15: 1135-1147.

Carrasco, A.R., Ferreira, O., Matias, A., Freire, P., 2012. Flood hazard assessment and management of fetch-limited coastal environments, *Ocean & Coastal Management*, 65: 15-25.

Coles, S., 2001. *An Introduction to Statistical Modeling of Extreme Values.*Springer, Berlin, 210pp.

Demerliac, M. A., 1974. Calcul du niveau moyen journalier. *Annales Hydrographiques du SHOM*, 5ème série, 2: 49–57.

Dodet, G. 2013. *Morphodynamicmodelling of a wave-dominatedtidal inlet: the Albufeiralagoon*, Ph.D. Dissertation, Université de La Rochelle, 181 pp.

Dodet, G., Bertin, X., Taborda, R., 2010.Wave climate variability in the North-East Atlantic Ocean over the last six decades.*Ocean Modeling*, 31 (3-4), 120-131.

Eliot, M., 2010. Influence of interannual tidal modulation on coastal flooding along the Western Australian coast, *Journal of Geophysical Research*, 115/C11013, DOI: 10.1029/2010JC006306.

Fanjul, E.A., Gomez, B.P., Carretero, J.C., Arevalo, I.R.S., 1998. Tide and surge dynamics along the Iberian Atlantic coast, *OceanologicaActa*, 21/2: 131-143.

Fortunato, A.B., Pinto,L. Oliveira,A., FerreiraJ.S., 2002. Tidally generated shelf waves off the western Iberian coast, *Continental Shelf Research*, 22/14: 1935-1950

Fortunato, A.B., Bruneau,N.,Azevedo, A.,Araújo, M.A.V.C.,Oliveira, A.,2011. Automatic improvement of unstructured grids for coastal simulations, *Journal of Coastal Research*, Special Issue 64: 1028-1032.

Fortunato, A.B., Rodrigues, M.,Dias, J.M.,Lopes, C.,Oliveira,A.,2013. Generating inundation maps for a coastal lagoon: A case study in the Ria de Aveiro (Portugal), *Ocean Engineering*, 64: 60-71.

Freitas, J.G., Dias, J.A., 2013. 1941 windstorm effects on the Portuguese Coast. What lessons for the future? *Journal of Coastal Research*, Special Issue 65: 714-719. DOI: 10.2112/SI65-121.

Guerreiro, M., Fortunato, A.B., Freire, P., Rilo, A., Taborda, R., Freitas, M.C., Andrade, C., Silva, T., Rodrigues, M., Bertin, X., Azevedo, A., 2015. Evolution of the hydrodynamics of the Tagus estuary (Portugal) in the 21st century.*Revista de Gestão Costeira Integrada /JournalofIntegratedCoastal Zone Management*, 15/1: 65-80.DOI: 10.5894/rgci515.

Haigh, I.D., Nicholls, R., Wells, N., 2010. A comparison of the main methods for estimating probabilities of extreme still water levels.*Coastal Eng*. 57, 838–849.

Haigh, I.D., MacPherson, L.R., Mason, M.S., Wijeratne, E.M.S., Pattiaratchi, C.B., Crompton, R.P., George, S., 2014a.Estimating present day extreme water level exceedance probabilities around the coastline of Australia: tropical cyclone-induced storm surges.*Climate Dynamics*, 42/1-2: 139-157.

Haigh, I.D., Wijeratne, E.M.S., MacPherson, L.R., Pattiaratchi, C.B., Mason, M.S., Crompton, R.P., George, S., 2014b. Estimating present day extreme total water level exceedance probabilities around the coastline of Australia: tides, extra-tropical storm surges and mean sea level. *Climate Dynamics*, 42/1-2: 121-138.

Holman, R.A., 1986. Extreme value statistics for wave run-up on a natural beach.*Coastal Engineering*, 9: 527-544.

Horsburgh, K.J., Wilson, C., 2007. Tide-surge interaction and its role in the distribution of surge residuals in the North Sea, *Journal of Geophysical Research*, 112, C08003.

Idier, D., Dumas, F., Muller, H., 2012. Tide-surge interaction in the English Channel,

704   *NaturalHazards and Earth System Science*, 12: 3709-3718.

705   Lopes, C.L., Dias, J.M., 2015. Assessment of flood hazard during extreme sea levels in a
706   tidally dominated lagoon, *Natural Hazards*, 77:1345-1364

707   Marcos, M., Chust, G. Jordà, G., Caballero,A., 2012. Effect of sea-level extremes on the
708   western Basque coast during the 21st century, *Climate Research*, 51:237-248.

709   Mazas, F., Kergadallan, X.,Garat,P.,Hamm, L., 2014.Applying POT methods to the revised
710   Joint Probability Method for determining extreme sea levels, *Coastal Engineering*, 91:
711   140-150.

712   Menendez, M., Woodworth, P.L. 2010.Changes in extreme high water levels based on a
713   quasi-global tide-gauge data set, *Journal of Geophysical Research Oceans*, 115.

714   Nicholls, R.J., Wong, P.P., Burkett, V.R., Codignotto, J.O., Hay, J.E., McLean, R.F.,
715   Ragoonaden, S., Woodroffe, C.D., 2007. Coastal systems and low-lying areas. Climate
716   Change 2007: Impacts, Adaptation and Vulnerability. Contribution of Working Group II to
717   the Fourth Assessment Report of the Intergovernmental Panel on Climate Change, M.L.
718   Parry, O.F. Canziani, J.P. Palutikof, P.J. van der Linden and C.E. Hanson, Eds.,
719   Cambridge University Press, Cambridge, UK, 315-356.

720   Pairaud, I.L., Lyard, F., Auclair, F., Letellier, T., Marsaleix, P., 2008. Dynamics of the semi-
721   diurnal and quarter-diurnal internal tides in the Bay of Biscay. Part 1: barotropic tides.
722   *Continental Shelf Research*, 28: 1294-1315.

723   Pereira, C., Coelho, C., 2013. Coastal risk maps due to wave action, *Revista de
724   GestãoCosteiraIntegrada / Journal of Integrated Coastal Zone Management*, 1371: 27-
725   43 (in Portuguese).

726   Perini, L., Calabrese, L., Salerno, G., Ciavola, P., Armaroli, C., 2015. Evaluation of coastal
727   vulnerability toflooding: comparison of two differentmethodologies adopted by theEmilia-
728   Romagna Region (Italy), *Natural Hazards and Earth System Science Discussions*, 3:
729   4315–4352. DOI:10.5194/nhessd-3-4315-2015

730   Pinto, L., Fortunato, A.B., Zhang,Y., Oliveira, A., Sancho, F.E.P., 2012. Development and
731   validation of a three-dimensional morpho-dynamic modelling system for non-cohesive
732   sediments, *Ocean Modelling*, 57-58: 1-14.

733   Pond, S.,Pickard, G.L., 1998.*Introductory dynamical oceanography*, Butterworth-Heinmann.

734   Pugh, D., Vassie, J., 1980. Applications of the joint probability method for extreme sea-level
735   computations.*Proc. Inst. Civ. Eng.* 69, 959–975.

736   Quevauviller, P., 2011.Adapting to climate change: reducing water-related risks in Europe –
737   EU policyand research considerations, *Environmental Science and Policy*, 14: 722–729.

738   Rego, J.L., Li, C., 2010. Nonlinear terms in storm surge predictions: Effect of tide and shelf
739   geometry with case study from Hurricane Rita, *J. Geophys. Res.*, 115, C06020,
740   doi:10.1029/2009JC005285.

741   Rodrigues, M., Oliveira,A., Queiroga,H., Fortunato, A.B., Zhang, Y.J., 2009). Three-
742   dimensional modeling of the lower trophic levels in the Ria de Aveiro (Portugal),
743   *Ecological Modelling*, 220/9-10: 1274-1290

744   Rodrigues, M., Oliveira, A.,Guerreiro, M.,Fortunato, A.B.,Menaia, J.,David, L.M.,Cravo,
745   A.,2011. Modeling fecal contamination in the Aljezur coastal stream (Portugal), *Ocean
746   Dynamics*, 61/6: 841-856

Rodrigues, M., Oliveira, A., Queiroga, H., Brotas, V., 2012. Seasonal and diurnal water quality and ecological dynamics along a salinity gradient (Mira channel, Aveiro lagoon, Portugal),*Procedia Environmental Sciences*, 13:899-918.

Roland, A., Zhang, Y.J., Wang, H.V., Meng, Y., Teng, Y.-C., Maderich, V., Brovchenko, I., Dutour-Sikiric, M., Zanke, U., 2012. A fully coupled 3D wave-current interaction model on unstructured grids, *Journal of Geophysical Research*, 117, C00J33, DOI: 10.1029/2012JC007952.

Saha, S., Moorthi, S., Pan, H.-L., Wu, X., Wang, J., Nadiga, S., et al. 2010. The NCEP Climate Forecast System Reanalysis. *Bulletin of the American Meteorological Society*, *91*(8), 1015–1057. doi:10.1175/2010BAMS3001.1

Serafin, K.A., Ruggiero, P., 2014. Simulating extreme total water levels using a time-dependent, extreme value approach, *Journal of Geophysical Research: Oceans*, 119/9: 6305-6329.

Simon, B., 2007. La marée océanique côtière. Collection "Synthèses". Institut Océanographique, 433 pp.

Stockdon, H.F., Holman, R.A., Howd, P.A., Sallenger Jr., A.H., 2006. Empirical parameterization of setup, swash and runup.*Coastal Engineering*, 53: 573-588.

Stopa, J.E., Cheung, K.F., 2014. Intercomparison of wind and wave data from the ECMWF Reanalysis Interin and the NCEP Climate Forecast System Reanalysis, *Ocean Modeling*, 75: 65-83.

Tavares, A.O., Santos, P.P., Freire, P., Fortunato, A.B., Rilo, A., Sá, L., 2015. Flooding hazard in the Tagus estuarine area: the challenge of scale in vulnerability assessments.*Environmental Science & Policy*, 5 1: 238-255. DOI: 10.1016/j.envsci.2015.04.010.

Tawn, J.A., 1988. An extreme value theory model for dependent observations.*J. Hydrol*. 101, 227–250.

Tawn, J., 1992. Estimating probabilities of extreme sea-levels.*Appl. Statist*. 41, 77–93.

Tawn, J.A., Vassie, J.M., 1989. Extreme sea levels: the joint probability method revisited and revised, *Proceedings of the Institution of Civil Engineers*, Part 2, 87: 429-442.

Weiss, J., Bernardara, P., Benoit, M., 2014. Modeling intersite dependence for regional frequency analysis of extreme marine event, *Water Resources Research*, 50: 5926–5940, doi:10.1002/2014WR015391

Wöppelmann, G., Pouvreau, N., Coulomb, A., Simon, B., Woodworth, P.L., 2008. Tide gauge datum continuity at Brest since 1711: France's longest sea-level record, *Geophysical Research Letters*, 35: L22605.

Zhang, H., Sheng, J., 2013. Estimation of extreme sea levels over the eastern continental shelf of North America, *Journal of Geophysical Research: Oceans*, 118: 6253-6273.

Zhang, Y.-L., Baptista, A.M., 2008. SELFE: A semi-implicit Eulerian-Lagrangian finite-element model for cross-scale ocean circulation. *Ocean Modelling*, 21/3-4: 71-96.

Zhang, Y., Witter, R., Priest, R., 2011. Tsunami–tide interaction in 1964 Prince William Sound tsunami.*Ocean Modelling*, 40/3-4, 246-259.
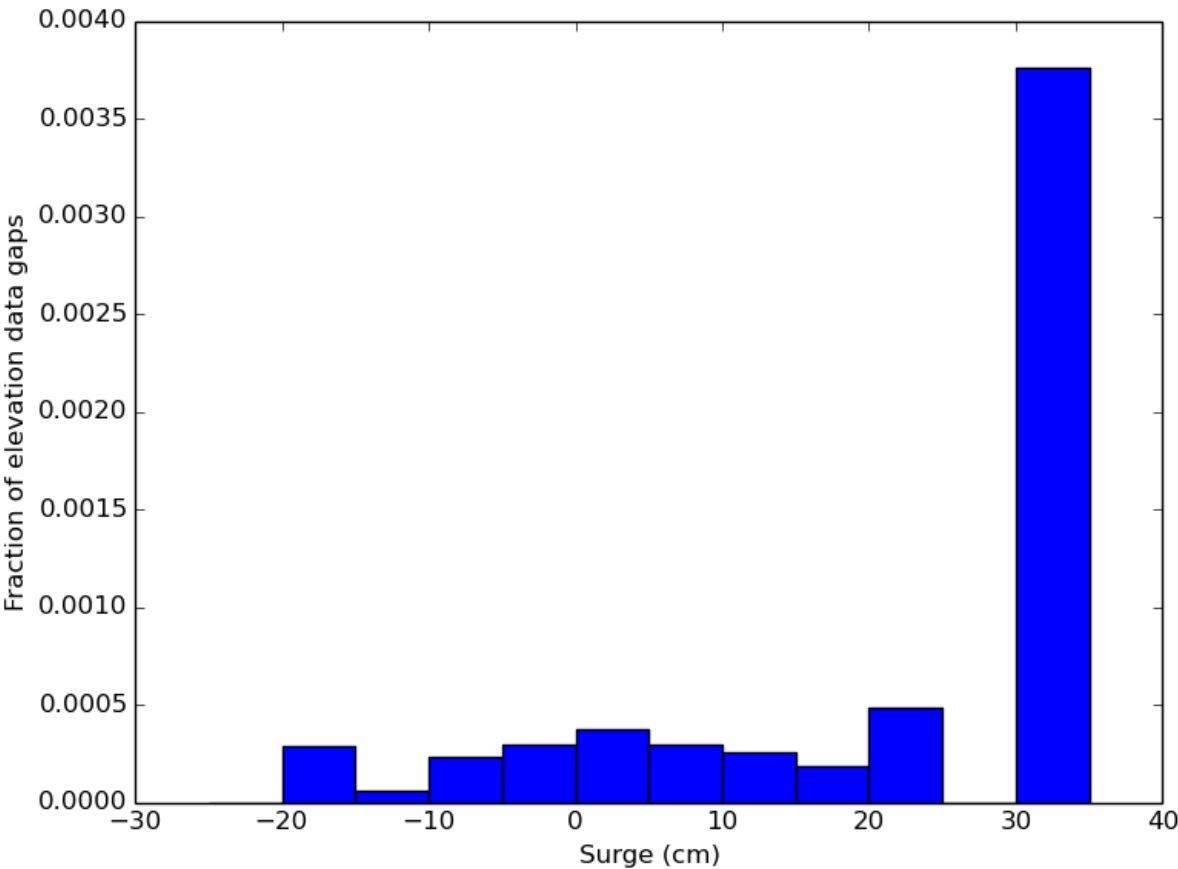
788 **Figures**

789

790
791 Figure 1. Fraction of the beginning of data gaps in the Cascais for different ranges of low frequency surges. The surges
792 were obtained by filtering the results of water elevations obtained with the regional model described below with a
793 Demerliac filter to remove daily and higher frequencies. Results suggest that data gaps occur more frequently during
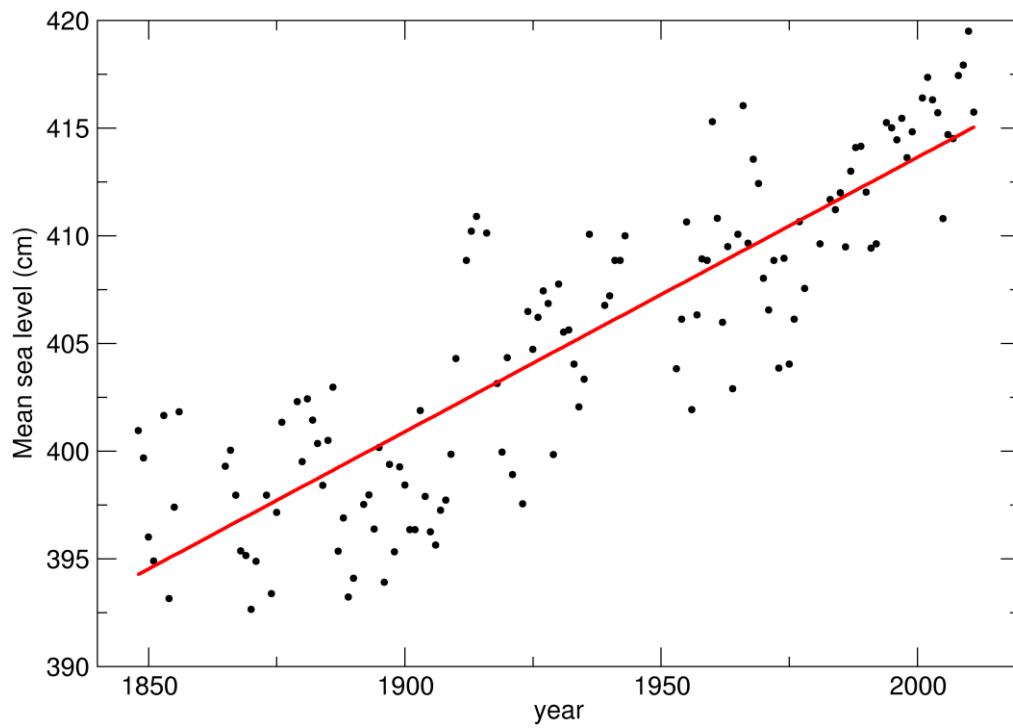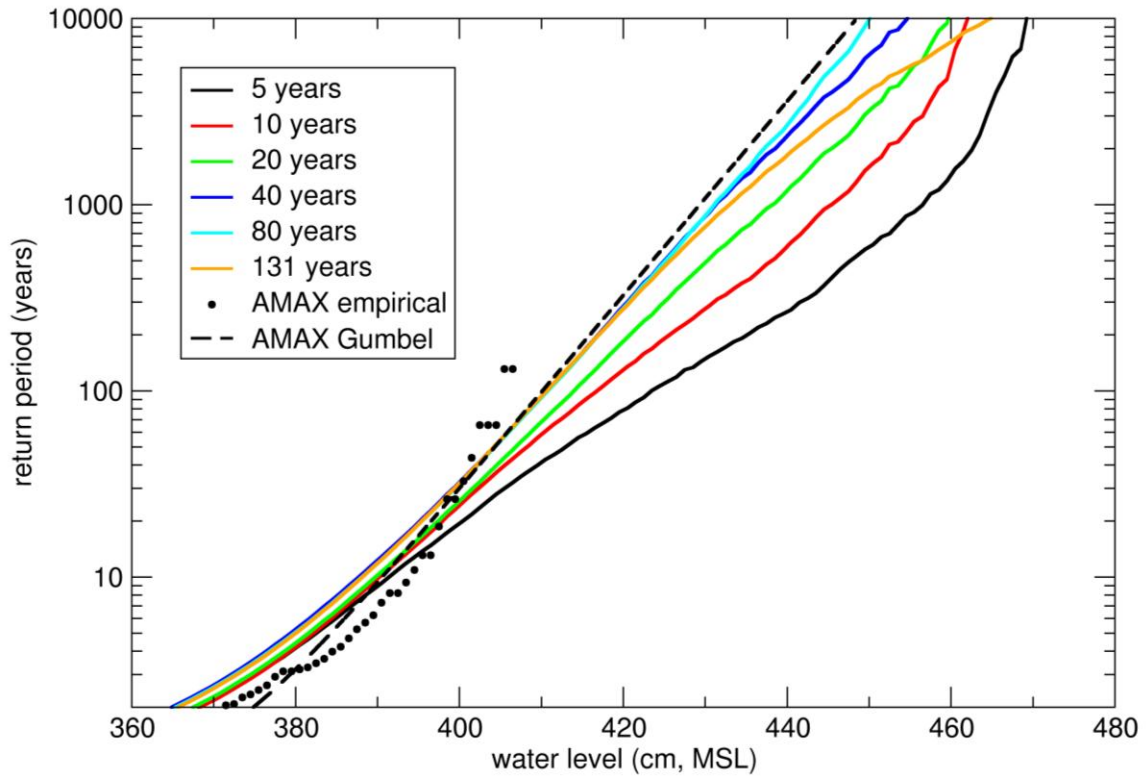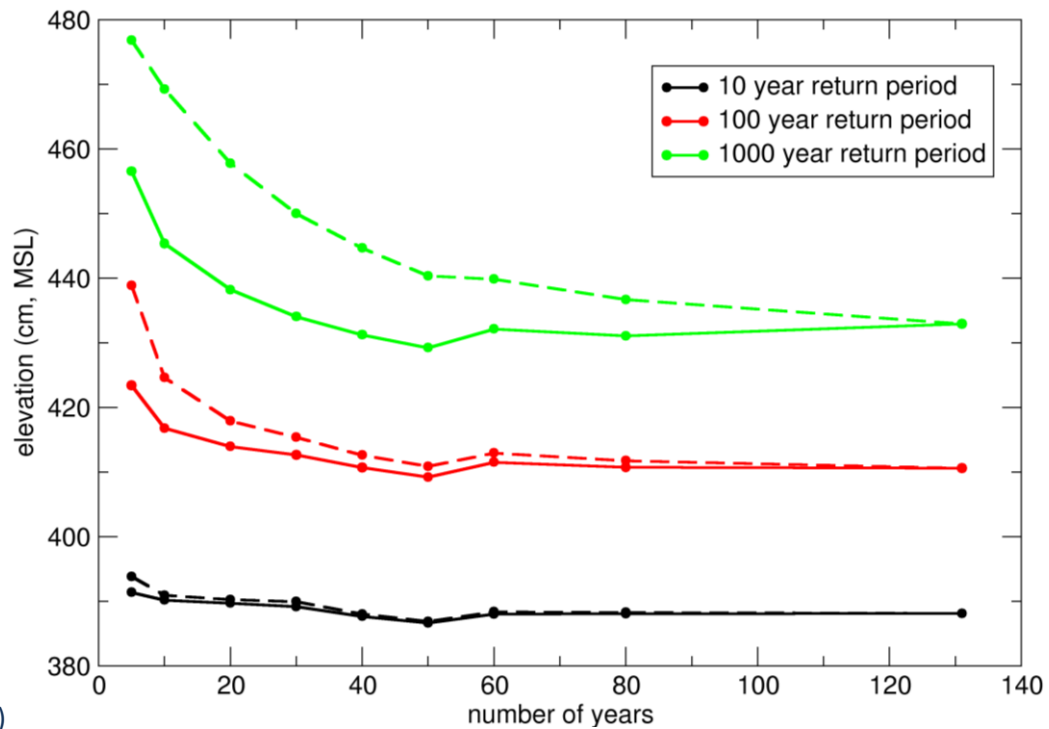794 periods with extreme events. Data spans the period 1977-2010.

795
796   **Figure 2.Long-term variability of the MSL at Brest, with a linear trend of 1.27 mm/year.**

797

798   a)

799   b)

800   **Figure 3. Convergence analysis: a) return period as a function of the maximum elevation for different numbers of years**
801   **of data; results from the direct application of the AMAX method to the observations are included for comparison; b)**
802   **convergence of the maximum elevation for return periods of 10, 100 and 1000 years. The dashed lines were computed**
803   **including data from 1987, the year with the maximum registered storm surge at Brest.**
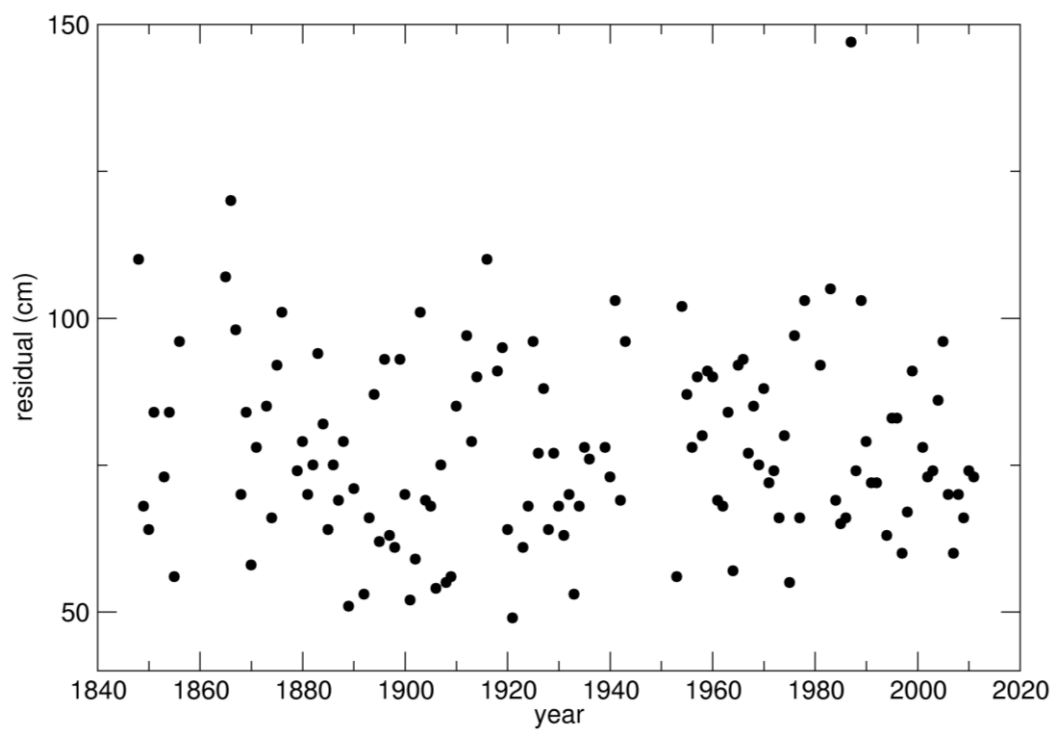
804
805   **Figure 4.Yearly maxima of residuals at Brest. The storm of 1987 stands out.**

806
807
808
809
810
811
812

813   a)

814   b)
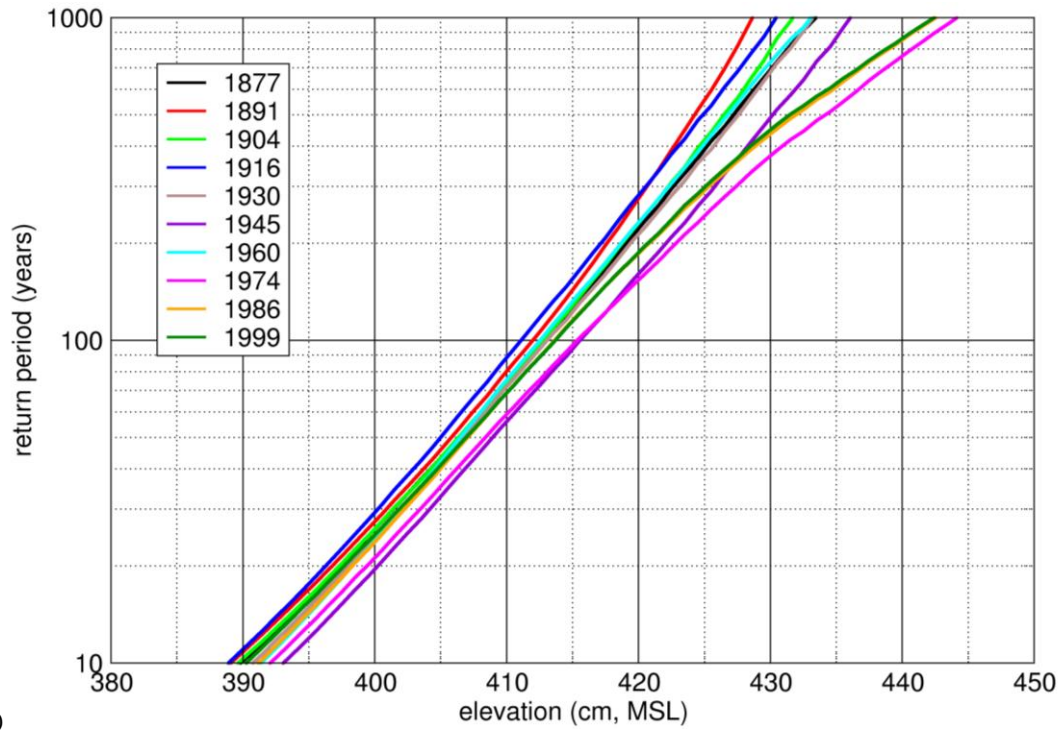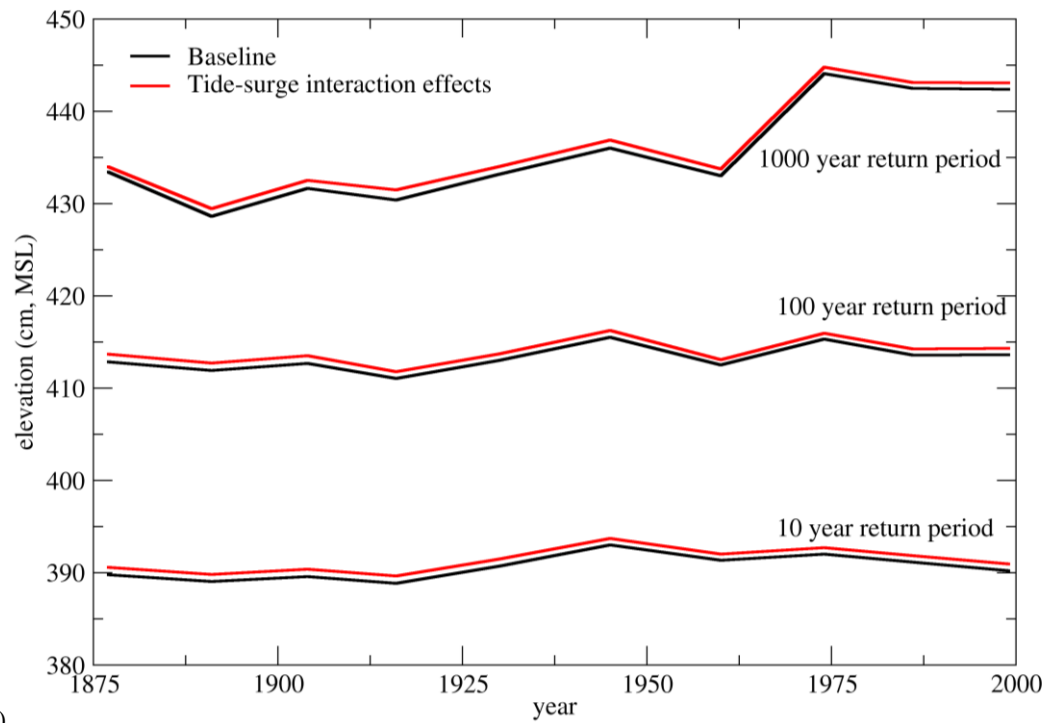
815 **Figure 5. Evolution of extreme sea elevations for different return periods determined using a sliding window with 41**
816 **years: a) return period as a function of the maximum elevation; b) evolution of the maximum elevation for selected**
817 **return periods and effect of tide-surge interactions.**

818
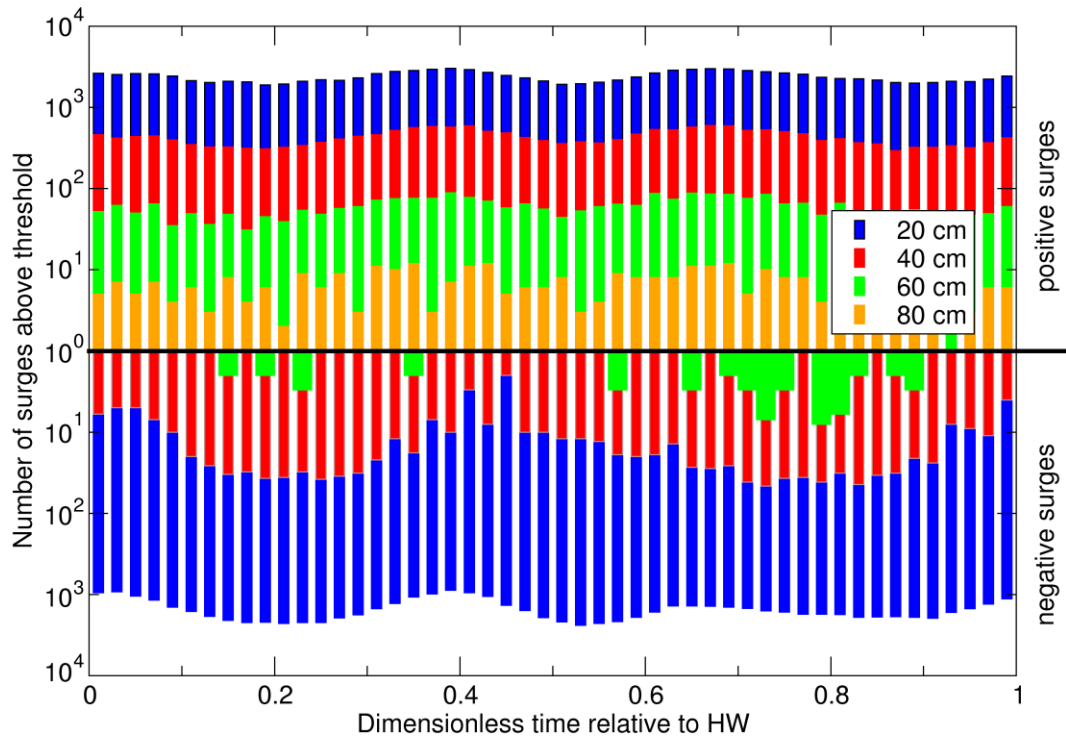
Figure 6. Illustration of tide-surge interactions at Brest for the 131 years analyzed. The horizontal axis represents the time between two consecutive high water tides. The upper (lower) bars represent the number of positive (negative) surges above a given threshold.
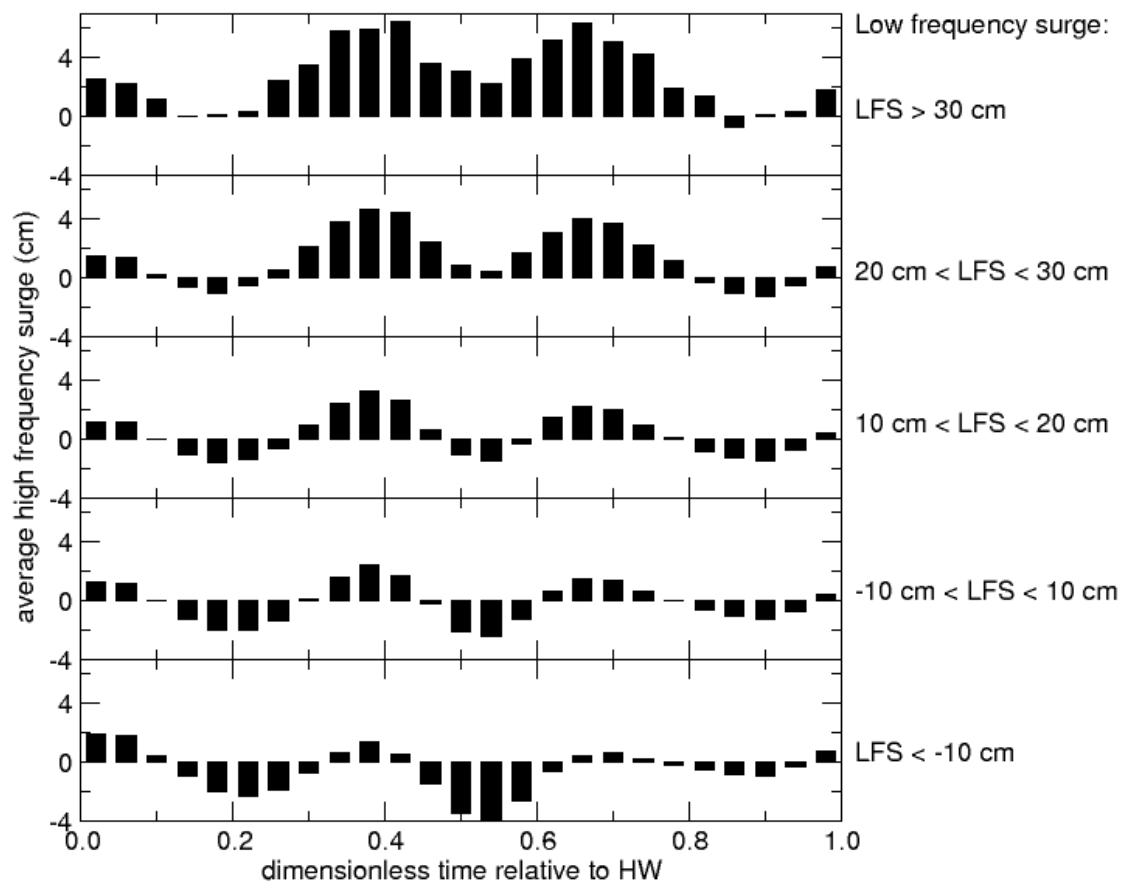
Figure 7. Average surge as a function of the tidal phase (horizontal axis) and low frequency surge (LFS, obtained by
applying a Demerliac filter to the observations).
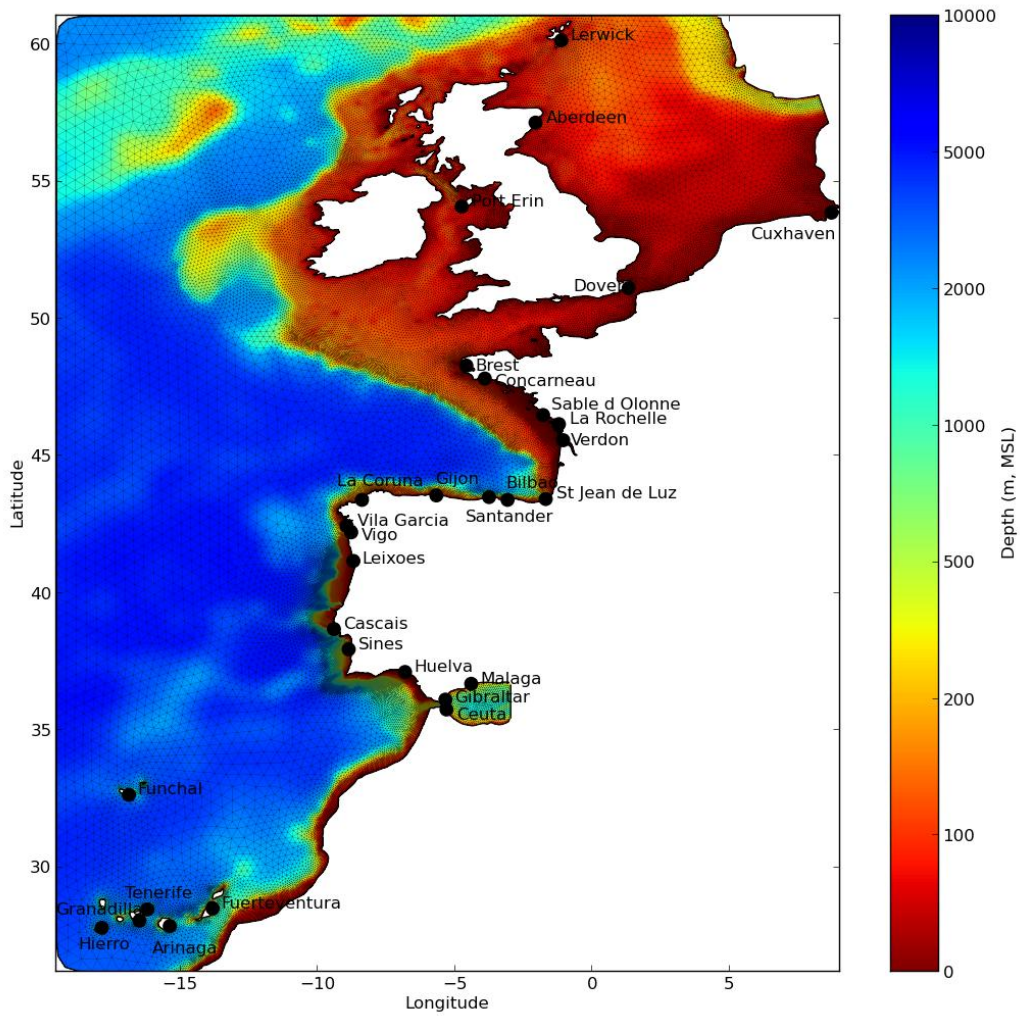
826
827
828   **Figure 8.Finite element grid, bathymetry and tidal stations.**

829
830

831   a)

832   b)

833 c)

834 d)
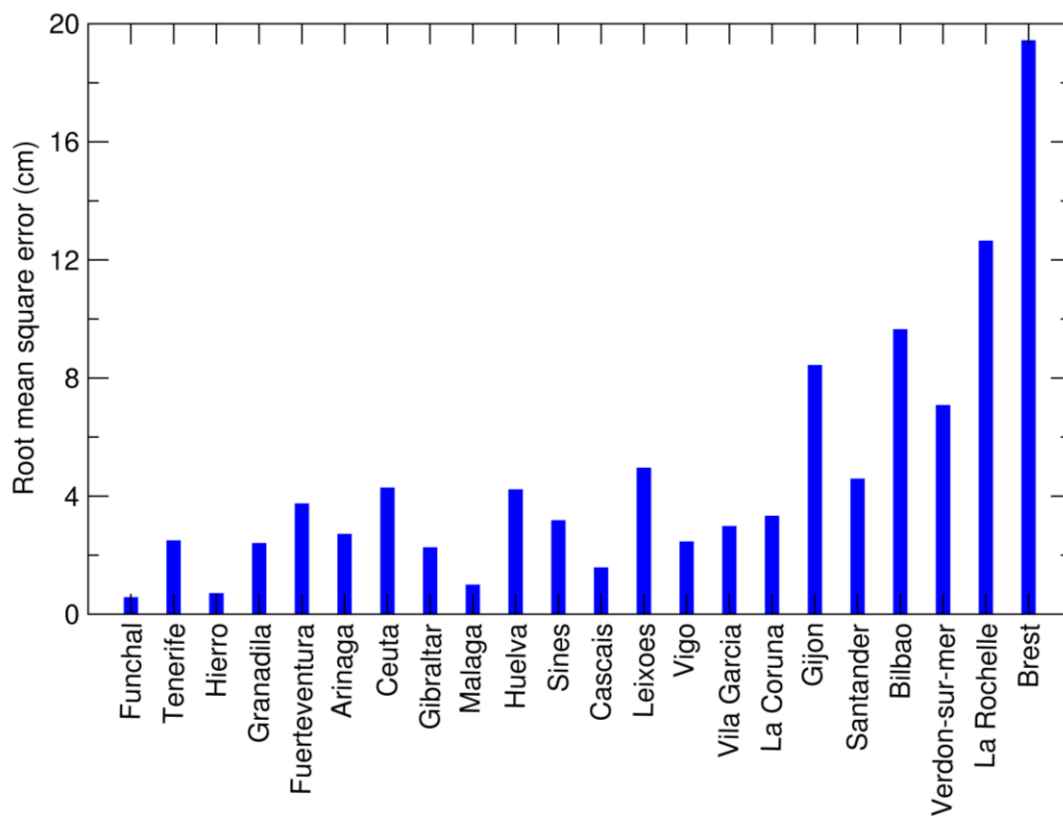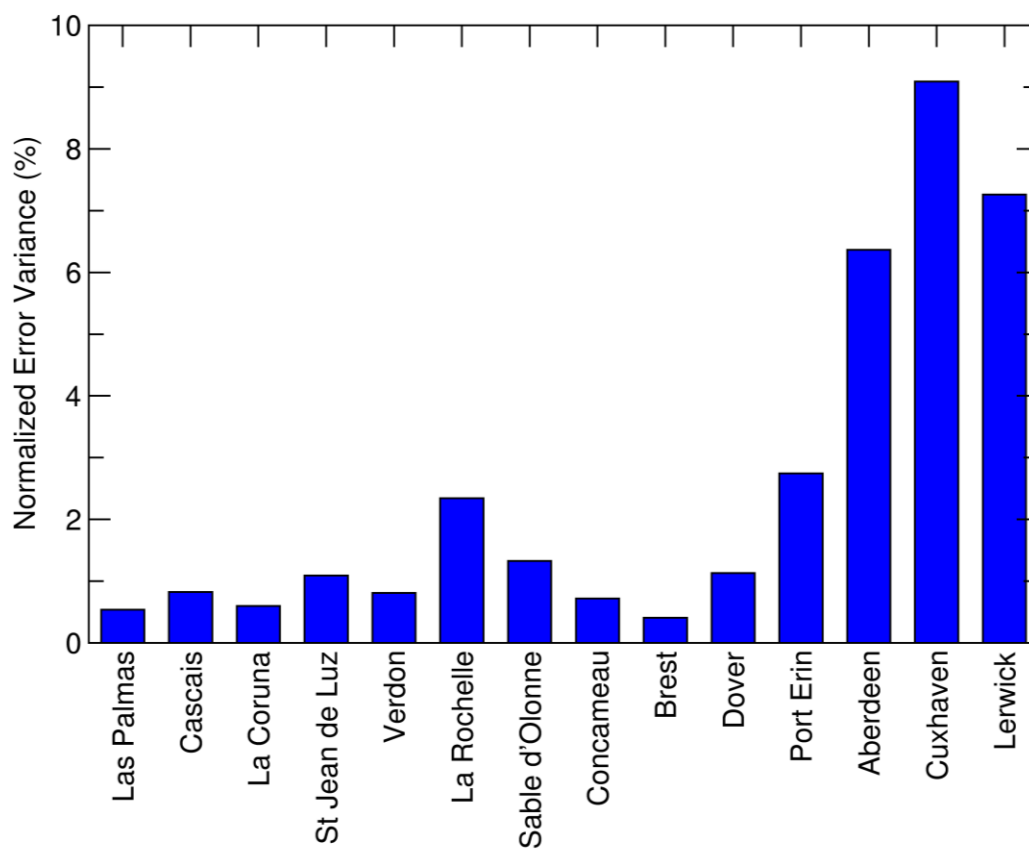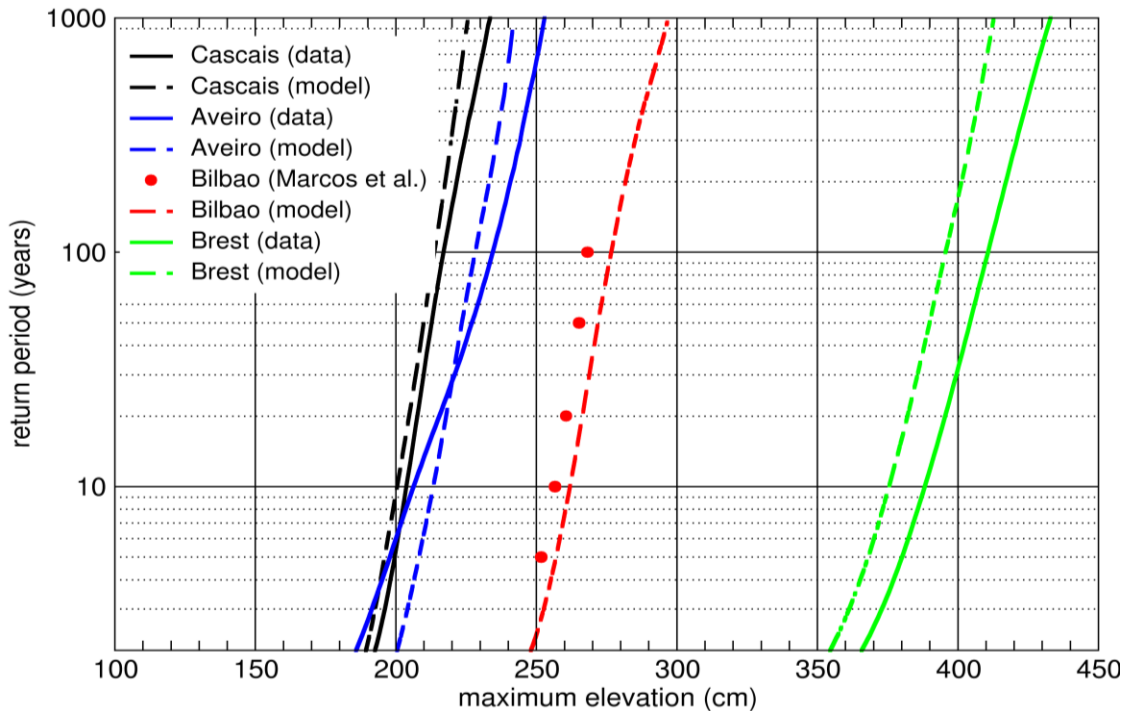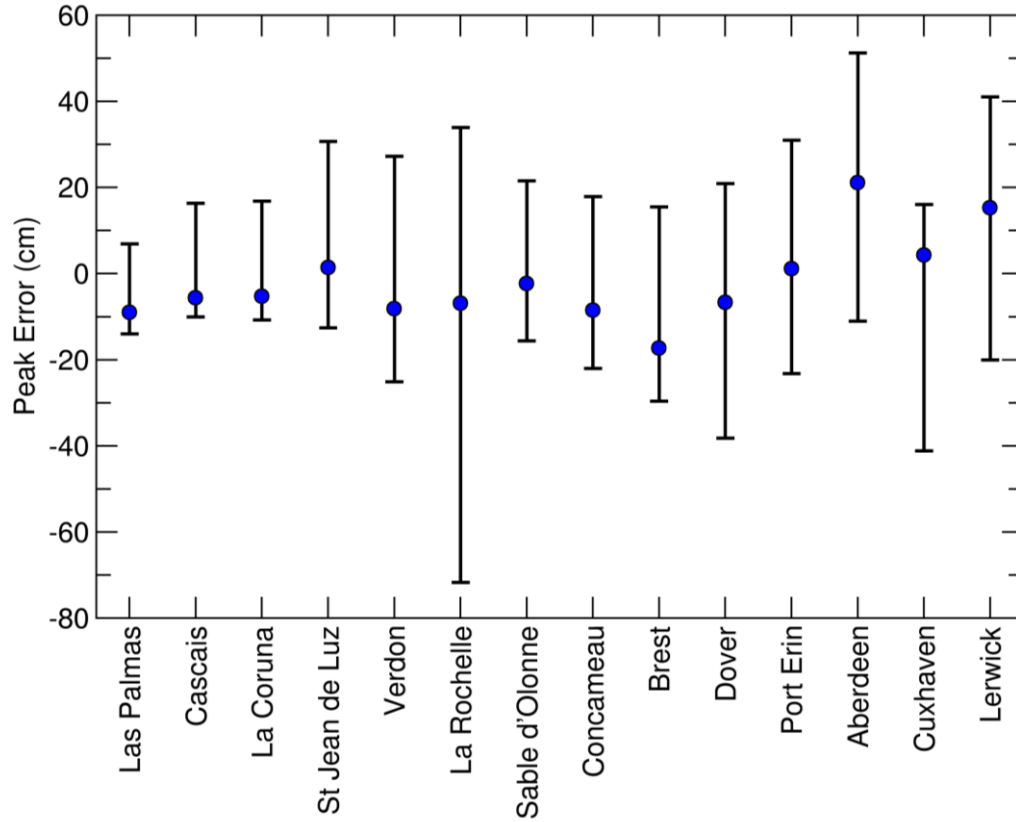
835 **Figure 9. Model validation: a) root mean square errors of the tidal model for the 5 major constituents (M2, S2, N2, O1,**
836 **K1); b)normalized error variance; c) peak errors at various stations during the 2009-2010 winter;the peak error range**
837 **indicates the maximum positive and negative differences between the observed and the modeled high tides; d)**
838 **comparison of the return periods of extreme sea levels computed with the present model with those from a different**
839 **model (Bilbao, from Marcos et al., 2012) or data (Cascais, from Guerreiro et al., 2015; Aveiro, from Fortunato et al.,**
840 **2013 and Brest).**
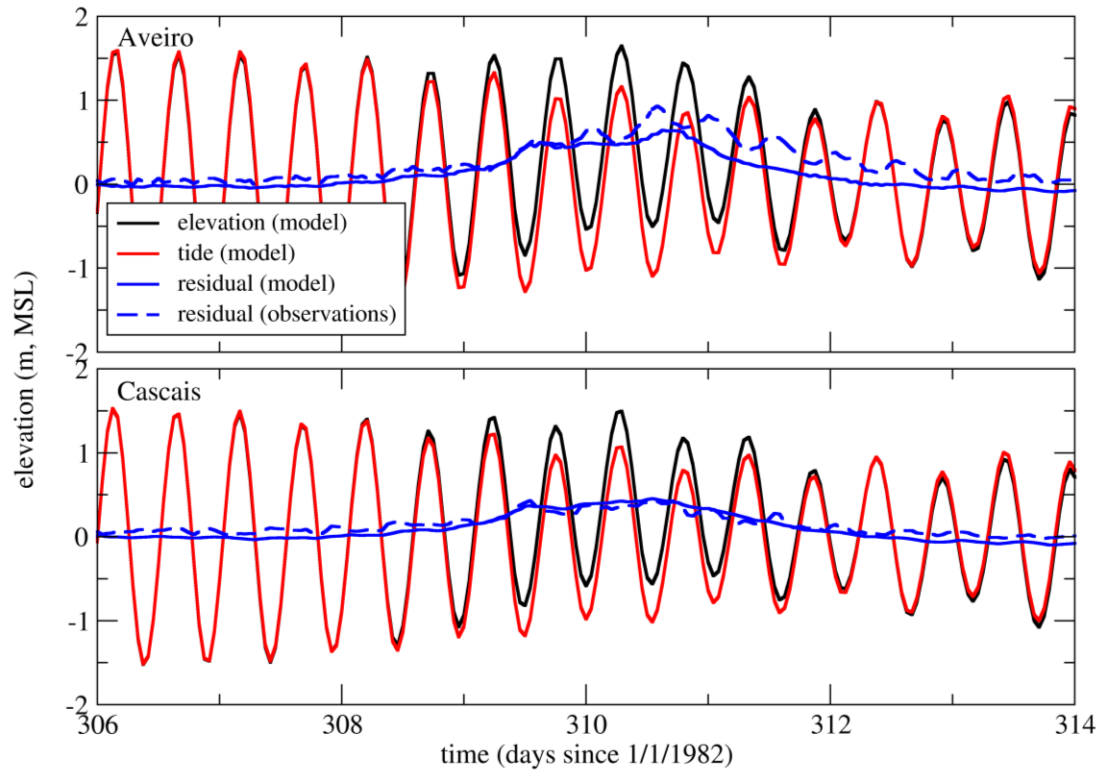
841
842 **Figure 10.Simulation of a storm surge in November 1982. Residuals obtained from observations were computed by**
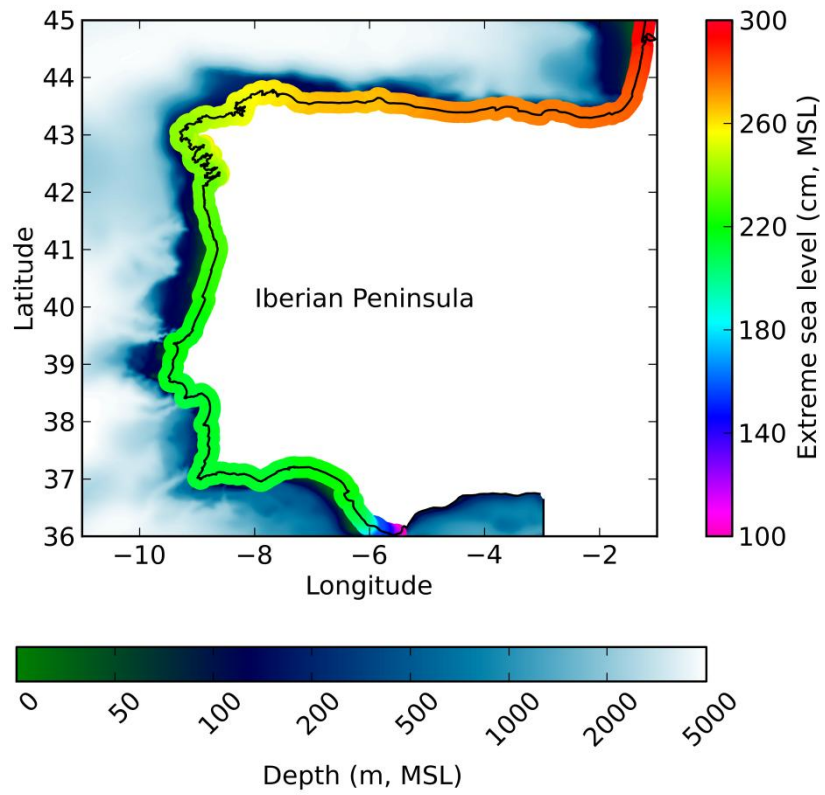843 **Fortunato *et al*. (2013) and Guerreiro*et al*. (2015) for Aveiro and Cascais, respectively.**

844
845   **Figure 11. Extreme sea levels along the Iberian Atlantic coast for a return period of 100 years.**
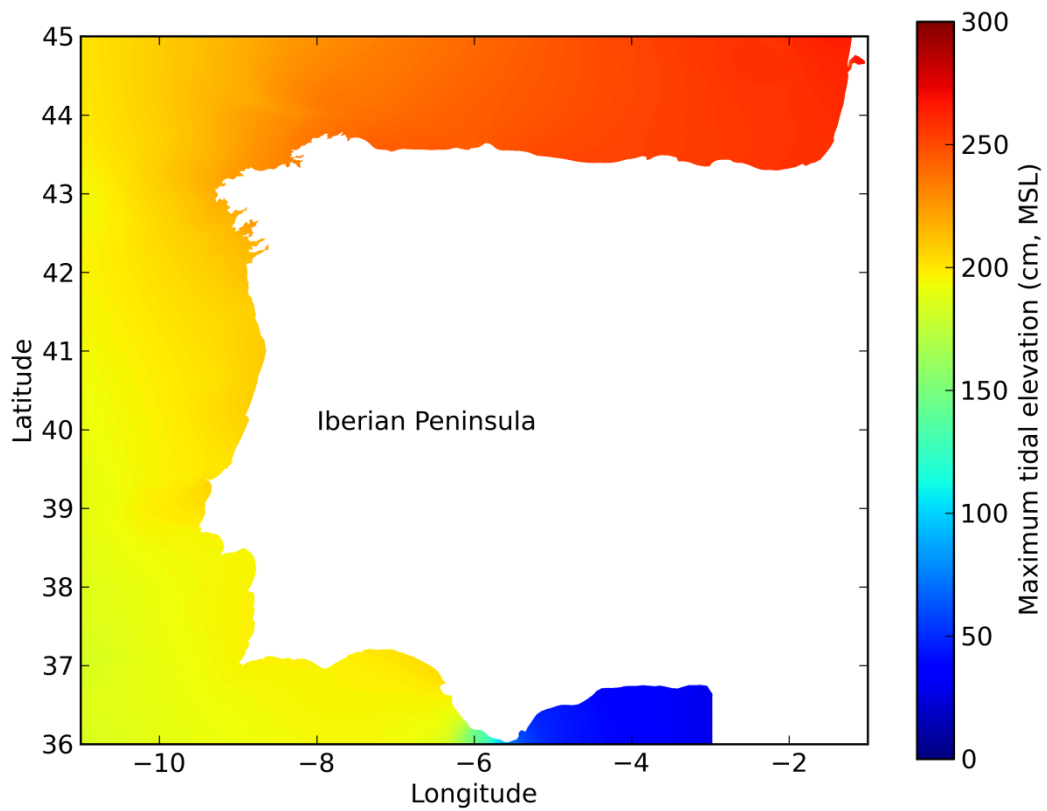
846

847
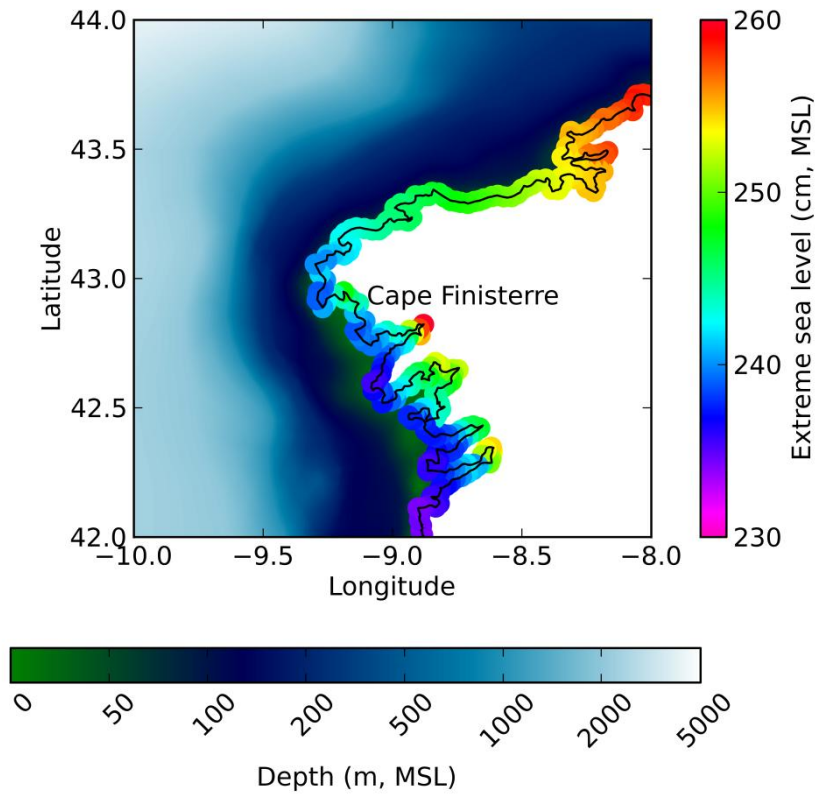848   **Figure 12.Maximum tidal elevations for a 1 year simulation.**

849
850

851
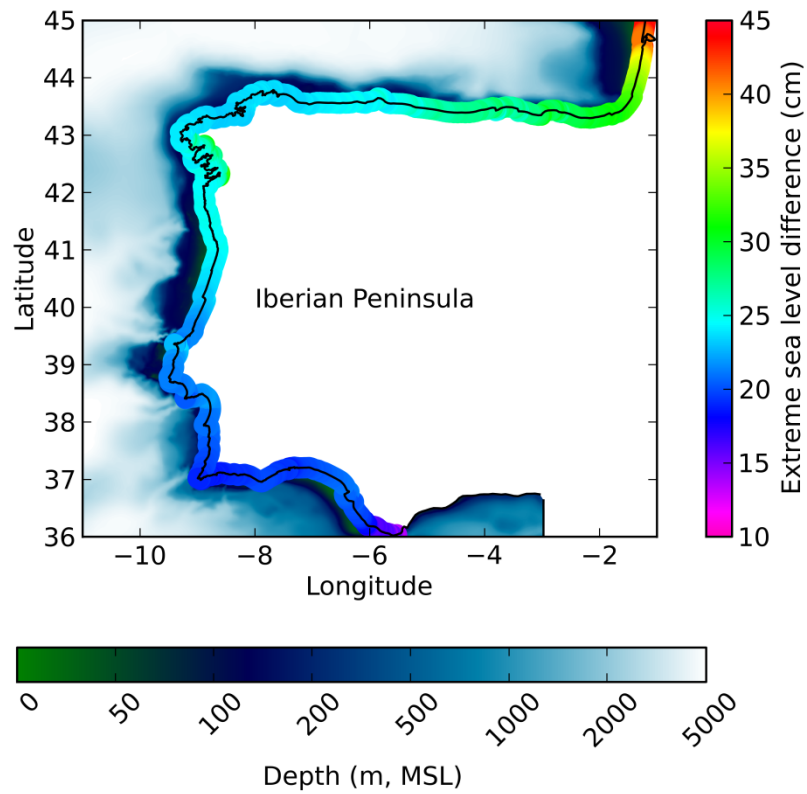852   **Figure 13.Extreme sea levels in the north-western Iberian Atlantic coast for a return period of 100 years.**

853

854
855
856   **Figure 14.Difference between the extreme sea levels for return periods of 1000 and 20 years.**
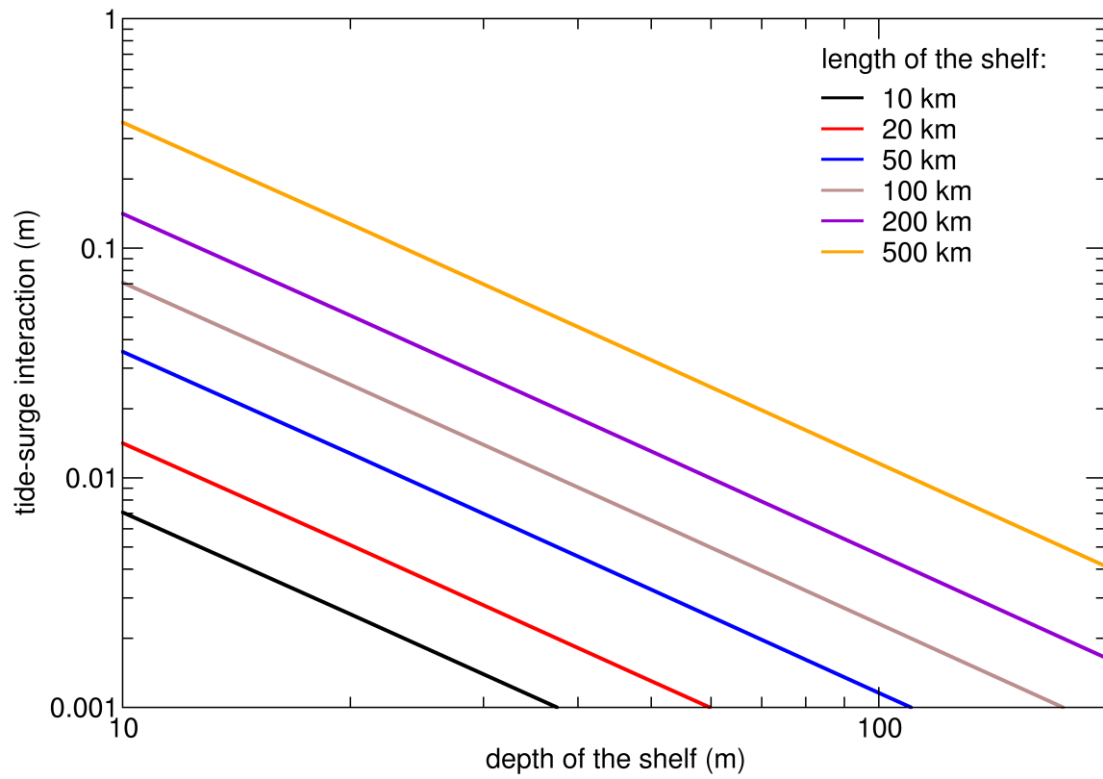
857

858

Figure A. 1. Estimation of tide-surge interaction effects due to changes in tidal celerity associated with surges. The tidal amplitude is taken as 2 m, the surge as 0.5 m, and the tidal period as 12 hours.
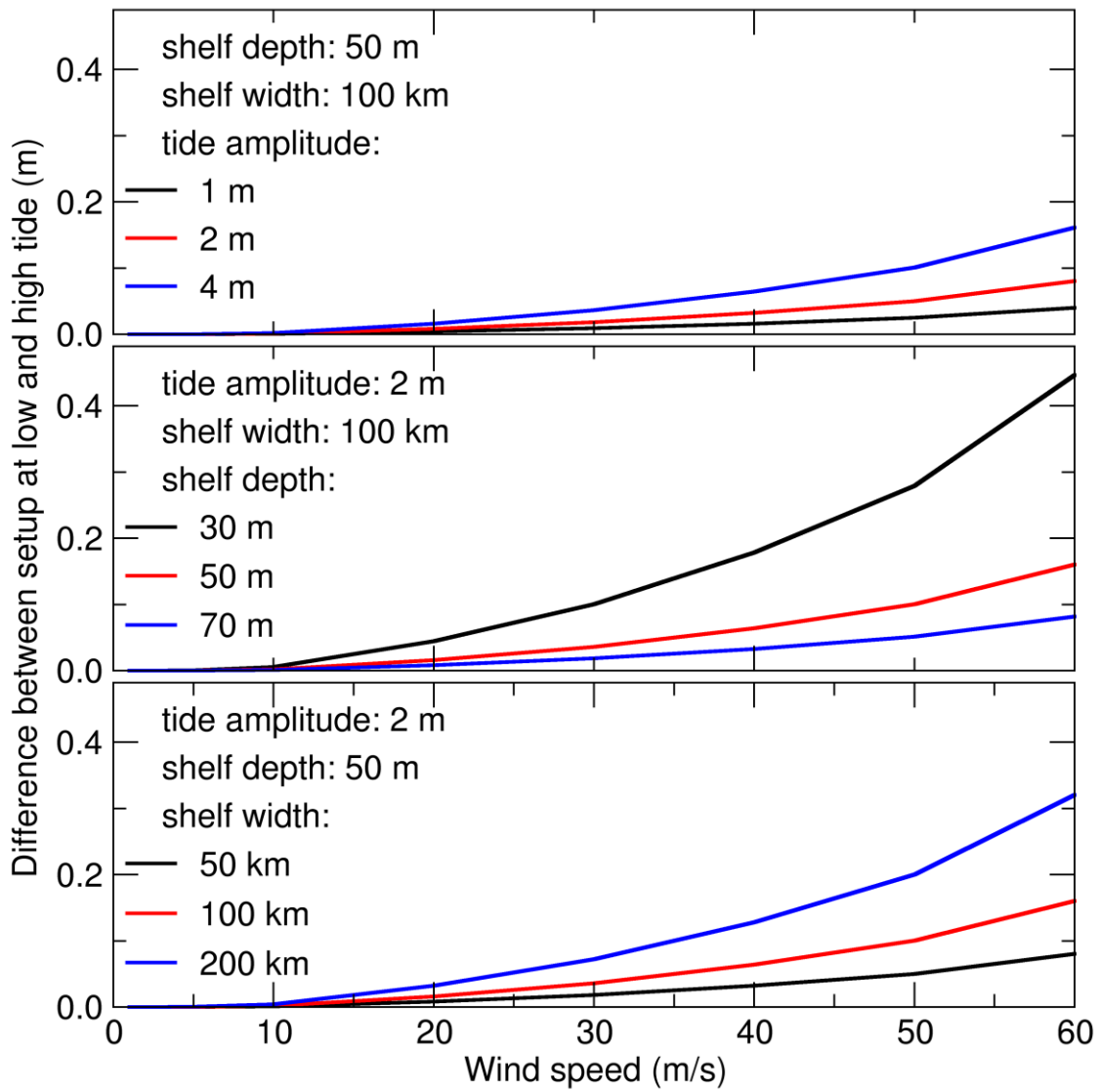
862
863 **Figure A. 2. Estimation of tide-surge interaction effects due to the different impact on wind setup at high and low tide.**

864